University of Naples Federico II

School of Engineering

Department of Chemical Engineering, Materials and Industrial Production

Ph.D in Engineering of Materials and Structures

XXVI Cycle

BROWNIAN MOTION IN MICROMETRIC COMPLEX CONFINEMENT

Ph.D Thesis

Francesco Gentile

TUTOR	COORDINATOR
Prof. Dr Paolo A. Netti	Prof. Dr Giuseppe Mensitieri

April 2014

Acknowledgements

A mio figlio Michele e mia moglie Anna.

Alla mia famiglia , a Mauro, Ilaria e Giovanni.

INDEX

1 CHAPTER: BROWNIAN DIFFUSION

2CHAPTER:

HINDERED BROWNIAN DIFFUSION IN SQUARE-SHAPED GEOMETRIES: THE DIHEDRAL EDGE EFFECT.

1 CHAPTER: BROWNIAN DIFFUSION

1 INTRODUCTION

Diffusion of colloidal particles is a very suggestive topic for industrial applications and biological understanding.

The fundamental aspects of diffusion have had interest in a wide time window, more than a century and a half, and now continue to arouse curiosity. From the scientific point of view several branches were approached for this study: physics, chemistry, engineering, mathematic and biology.

This remarkable interest is certainly due to the fact that the phenomenon involves many aspects of the modern experiments and it is present in a wide range of technologies used in contemporary life.

The introduction of increasingly sophisticated experimental techniques has allowed the opportunity to validate theoretical conjectures made in the past opening at the same time new areas of research. Among these new frontiers, the diffusive behaviour of particles in complex geometries or in complex fluids, together with the effect of particle shape certainly remain to unravel.

1.1 HISTORICAL BACKGROUND

The phenomenon of diffusion is one of the most interesting aspects if you want to study the evolution of any system. Migrations and

redistribution of atoms, molecules or any kind agglomerates, are the mechanisms of structural evolutions and reorganization of matter. Thermodynamic aspects often play a central role and establish the conditions for which a given phenomenon takes place. Nonetheless Thermodynamics don't say much about velocity and the time evolution and reaction of the system. It's obvious that a kinetic consideration is the central core of the study of the diffusion.

The first experiments and theoretical approach of small particles diffusing in fluid systems date back to Adolf Fick in the half of nineteenth century; at that time he proposed the quantitative laws of diffusion.

A new approach of diffusion, supported by the introduction of a statistical concept, was presented by Albert Einstein at the turn of the nineteenth and early twentieth century in his PhD thesis; indeed he began analysing the previous observations of Brown in 1828 about the chaotic motion of diffusive micrometric particles of pollen which floated above the surface of an aqueous suspension. Einstein gave a rigorous mathematical treatment of this phenomenon.

The attention applied to the study of the diffusion of small particles with dimensions in the range of a few nanometres up to the micron scale is certainly worthy of note.

1.2 FICK'S LAW

Fick hypothesized that the diffusive behaviour could be described with a law similar to those which are used for the transport phenomena of current and heat conduction. He used the same mathematical

formalism of the Furier's law for the conduction of heat and the Ohm's law regarding the electricity.[1]

An ensemble of small particles dispersed or dissolved in a generic fluid is taken into account. The nature of this particle is not relevant, in fact they could be molecules or colloidal spheres (e.g. polystyrene beads of the order from 0.1 μm diameter to few microns size). The number is constant in time and any particle is a point located through an orthonormal Euclidian system of coordinate. Since a point like depiction of the particle is used, we are obliged to write their density, usually denoted by the mass to volume ratio, through the density operator $n(x,t)$:

$$n(x,t) = \sum_{\alpha} \delta(x - x_{\alpha}) \qquad (1)$$

In a classical system the variable x_{α}, inside a Dirac delta function, is the dynamical variable specifying the position of the particle α. Of course $n(x,t)$ can be interpreted as an operator[2]; indeed the ensemble average of this operator is the average density in x position

$$\langle n(x) \rangle \qquad (2)$$

In homogenous and isotropic fluids of course considering the density mean value independent of position x, the operator corresponds to an average density $n = N/V$[3].

In Fick diffusion the variation of the density in time is represented by the following differential equation[4]:

$$\frac{\partial n(x,t)}{\partial t} + \nabla \cdot j(x,t) = 0 \qquad (3)$$

it obeys a conservation law, where $j(x,t)$ is the particle current, in analogous at current in electrodynamics[5]:

$$j(x,t) = \sum_\alpha v_\alpha \, \delta(x - x_\alpha) \qquad (4)$$

product of the particle velocity

$$v_\alpha = \frac{\partial x_\alpha}{\partial t} \qquad (5)$$

and the density operator $n(x,t)$.

In thermodynamic equilibrium is intuitive to assume that there are no variations in density from one point to another of the system, and the current *j* of the particles has a zero value. In this case the average value of the operator density is independent of the position x_α the system and of the time *t* parameter. A generic perturbation acting on the system,(e.g. a force applied for a finite time, or a spontaneous fluctuation) moves the ensemble momentarily away from equilibrium state. The particles of the system will move to restore the equilibrium state and therefore a homogeneous density. It is logical to think that the only way to restore the equilibrium of the system is achieved through the motion of the particles; indeed a displacement will take place from their non-equilibrium position towards a new reorganization. This phenomenon is correlated with non uniform local density and produces a value of the particle current different from zero. If the density variation between two neighbouring points is small, the value of current *j* will be quite small. There is a strict proportionality between the density gradient and the particle current. This proportionally is known as Fick Law's[6]:

$$\mathrm{j} = -D\nabla n \qquad (6)$$

The minus sign in the second term of Fick's equation explains that particle current direction is opposite to the density gradient, in order to restore a homogeneous density. The proportionality constant D is the diffusion coefficient and it has unity of [length]^2/[time].

The Fick's law (6) can be inserted into the conservation law (3), obtaining the equation of diffusion[7]:

$$\frac{\partial n}{\partial t} = D\nabla^2 n \qquad (7)$$

representing the temporal dependence of diffusion process. This is a parabolic differential equation. The modes obtained by this equation are achieved by making this assumption[8]:

$$n(x,t) \sim e^{-i\omega t} \qquad (8)$$

Thus the resulting frequency is:

$$\omega = -iDq^2 \qquad (9)$$

where the wave number $q = 2\pi/\lambda$ is the modulation of the spatial density (*figure 1*).

In the frequency ω there's an imaginary part that accounts for an oscillating behaviour. Once substituted into equation (8) the imaginary oscillatory contribution vanish and the response of $n(x,t)$ to external forces, the non equilibrium boundary condition, will exponentially decay to zero in times of order $D^{-1}\lambda^2$, without oscillating[9].

To evaluate how the system evolves after a perturbation the diffusivity equation must be solved. This corresponds to understanding

the dynamic of the density operator. Taking two time instants t and t' and the relative density at positions x and x', an integral relationship expressed by the next equation can be observed:

$$n(x,t) = \int d^d x' G(x - x', t - t') n(x't') \qquad (10)$$

where the $G(x,t)$ is the Diffusion Green function[10]. This function satisfies the boundary condition

$$G(x, t = 0) = \delta(x - x') \qquad (11)$$

which for $t > 0$ satisfies the Diffusion Equation (7):

$$\frac{\partial G(x,t)}{\partial t} = -D\nabla^2 G(x,t) \qquad (12)$$

The solution of this equation is obtained applying the Laplace and Fourier transform in time and in space domain respectively[11]:

$$G(q,z) = \frac{1}{-iz + Dq^2} \qquad (13)$$

and

$$G(q,t) = \int_{-\infty+i\varepsilon}^{\infty+i\varepsilon} \frac{dx}{2\pi} e^{-izt} G(q,z) = e^{-Dq^2|t|} \qquad (14)$$

$$G(x,t) = \int \frac{d^d q}{(2\pi)^d} e^{-iqx} G(q,t) = \frac{1}{(4\pi D|t|)^{d/2}} \, e^{\frac{-|x|^2}{4D|t|}} \qquad (15)$$

According to this equation a particle located in x_0 will spread in time in a cloud diffused around the initial position. This cloud increases its

radius occupying a volume region proportional to the mean square radius

$$\langle |x|^2 \rangle = 2dD|t| \qquad (16)$$

where d corresponds to the system dimensionality (d=1,2,3)[12].

The last equation is obtained by solving the differential equation and will be used in the experimental section to connect the displacement (easily measurable experimentally) to the diffusion of particles in isotropic systems. Obviously in anisotropic systems some consideration will be revisited. There is another way to obtain the same equation, using a statistical approach of diffusion.

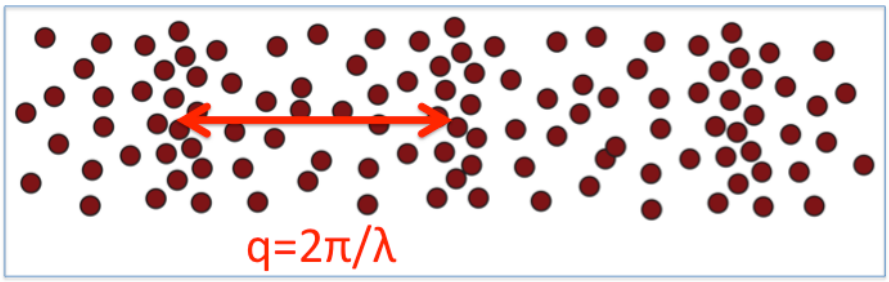

Figure 1: Spatial modulation od the density

1.3 EINSTEIN RELATION

The diffusion predicted by Fick's law fits very well in cases where there is no external potential; otherwise it is necessary to introduce some modifications. Take the case of a spherical particle ensemble, dispersed in a fluid with particles quite distant between each other. In this situation it is possible to assert that the particle-particle interactions

are negligible. The only potential derives from external forces which may act on the system, and the internal force interaction due to the collision with solvent molecules: the fluid motion is due to thermal agitation. In this way the effect of the fluid is to introduce an internal force; indeed if the particles have mass m and they move in the solvent, a viscous fluid, then a single sphere will be subject to a force proportional to its velocity, called friction force[13]:

$$f_{vis} = -\alpha v \qquad (17)$$

where $\alpha = 6\pi\eta a$ is a friction constant given by the Stokes's law, η is the viscosity of the fluid and a the radius of the particle. The friction constant α has the units of [mass]/[time], the viscosity η of [energy•time]/[Volume] and the radius of [length].

Of course if we are in steady state the internal force of the system, the force mentioned above, is in equilibrium with the external forces, and the resultant drift velocity of the particle will be:

$$v_D = \frac{1}{\alpha} f^{ext} \equiv -\frac{1}{\alpha} \nabla U \qquad (18)$$

where U is the external potential. This drift will originate a diffusion current:

$$j_D = n v_D \qquad (19)$$

that will be added to the diffusion current predicted by the Fick's law. The final diffusion current will be a sum of the above contributions:

$$j_{tot} = -D\nabla n + j_D = -D\nabla n + n\left(-\frac{1}{\alpha}\nabla U\right) \qquad (20)$$

In condition of thermodynamic equilibrium the total particle current is zero and the density value is governed by the Boltzmann relation[14]:

$$n_{eq} \sim e^{\frac{U(x)}{T}} \qquad (21)$$

The only way to satisfy this condition is that the diffusion coefficient is directly proportional to the temperature T of the system and inversely to a friction coefficient deriving by the Stokes's law:

$$D = \frac{T}{\alpha} = \frac{T}{6\pi\eta a} \qquad (22)$$

where:

$$D = \lim_{t\to\infty} \frac{\langle [x(t-x(0))]^2 \rangle}{2dt} = \lim_{t\to\infty} \frac{1}{2d}\frac{d}{dt}\langle [x(t-x(0))]^2 \rangle \quad (23)$$

This equation creates a relationship between the mean square displacement of the particle and the diffusion coefficient.

Another consequence of the pervious equation the diffusion coefficient and the viscosity of the system is the stokes Einstein relation[15]:

$$D = \frac{K_b T}{6\pi\eta a} \qquad (24)$$

where K_b = Boltzmann constant, η = viscosity of the system, and a=hydrodynamic radius of the sphere disusing in the fluid. This relation is the consequence of the

1.4 STATISTICAL APPROACH

Considering again a particle or a molecular system diffusing in a viscous medium, there are two ways to determine the dynamics of this problem. It could be possible in principle to write the equation of motion, the correct Hamiltonian of the whole system, and solving it exactly. Alternatively statistical approach could be used: all the possible trajectories of the particle could be considered, calculating afterwards the probability that a given displacement occurs for each of them. The first is an exact method but unpractical for big and complex (the number of the elements composing the system is bigger than 10^{20}), and also for small system it's computationally expensive. The second can produce an excellent approximation[16].

Instead of predicting the evolution of all individual particles, the probabilistic method is concerned only with the probability that a given event occurs. In this case we deal with macroscopic systems from a microscopic point of view. it is possible to observe how a system made up of particles exhibits a behaviour governed by the laws of classical mechanics. The achievement is to predict the macroscopic behaviour of the system in terms of the system's microscopic dynamics. Statistical mechanics moreover studies fluctuations from equilibrium values, an aspect which is not contemplated in the thermodynamic approach. These fluctuations go to zero when both the number of particles N and the volume V tend to infinity while the ratio $\rho=N/V$ remains finite, which is called the thermodynamic limit. In such limit the statistical mechanics reproduce exactly the laws of thermodynamics.

1.5 RANDOM WALK

In this paragraph particles diffusing in a viscous medium are considered. The concepts addressed will be developed in one dimension (along the x direction) even if these arguments can be extended to the three dimensional case. Both time and space are considered discrete. For each path considered, the origin of the x-axis is fixed in the start position. The particle starts at the origin and will do a leap a_0 to the right or to the left for each time step τ. The probability of it jumping to the right or to the left are p and q respectively, with $q = 1 - p$. For each step the particle collides with solvent molecules and changes its direction: this is a stochastic process and between the two successive events there is no temporal relationship. Each jump is independent of the previous one and each step could be considered as an independent path. If the problem is symmetric there's the same probability to jump to the right or to the left and so p=q=1/2. Otherwise an overall drift due to the fact that p≠q is present. The problem is called a random walk, also well known as the drunkard's walk[17].

In general after N total steps, the probability that a walker moves n_1 steps to the right and n_2 = N-n_1 steps to the left is given by the binomial distribution[16]:

$$P_N(n_1) = C_N(n_1)p^{n_1}q^{n_2} \qquad (25)$$

where

$$N = n_1 + n_2 \qquad (26)$$

and $C_N(n_1)$ is the degeneracy, the all independent ways to have n_1 steps on the right with N total steps[17]:

$$C_N(n_1) = \binom{N}{n_1} = \frac{N!}{n_1!(N-n_1)!} \qquad (27)$$

The total displacement will be a difference between the right step and the left step[16].

$$m = n_1 - n_2 \qquad (28)$$

and, in this case, we calculate the mean value of displacement[16]:

$$\langle m \rangle = \langle n_1 \rangle - \langle n_2 \rangle \qquad (29)$$

To get this value it's necessary evaluating $\langle n_1 \rangle$ before: a sum of different independent paths to obtain n_1 right steps, each weighted by its own probability[16]:

$$\langle n_1 \rangle = \sum_n n_1 P_N(n_1) = \sum_n n_1 C_N(n_1) p^{n_1} q^{n_2} \qquad (30)$$

This sum could be evaluated through the method of "generating function"[16]: considering a function Z(x,y), with x=p and y=q, representing the series expansion of Newton's binomial:

$$Z(x,y) \equiv \sum_{n_1}^{N} C_N(n_1) x^{n_1} y^{n_2} = (x+y)^N \qquad (31)$$

it's simple to demonstrate that[16]:

$$x\frac{\partial Z(x,y)}{\partial x}\Big|_{\substack{x=p\\Y=q}} = \sum_n n_1 C_N(n_1) x^{n_1} y^{n_2}|_{\substack{x=p\\Y=q}} \equiv \langle n_1 \rangle \qquad (32)$$

and so:

$$\langle n_1 \rangle \equiv x\frac{\partial Z(x,y)}{\partial x}\Big|_{\substack{x=p\\Y=q}} = Nx(x+y)^{N-1}|_{\substack{x=p\\Y=q}} = Np \qquad (33)$$

same is for $\langle n_2 \rangle$:

$$\langle n_2 \rangle \equiv y\frac{\partial Z(x,y)}{\partial y}\Big|_{\substack{x=p\\Y=q}} = Ny(x+y)^{N-1}|_{\substack{x=p\\Y=q}} = N \qquad (34)$$

therefore, after N steps, the mean value of displacement will be[16]:

$$\langle m \rangle = N(p-q) \qquad (35)$$

If the probability to jump on the right is the same on the left the mean value will be zero, but in statistical mechanics the value of fluctuation about the mean must be taken into account:

$$\langle (\Delta m)^2 \rangle = \langle (m - \langle m \rangle)^2 \rangle = \langle m^2 \rangle - \langle m \rangle^2 \qquad (36)$$

After substituting (26) in (28), it's obtained:

$$n_1 = \frac{m+N}{2} \qquad (37)$$

and so:

$$\langle(\Delta m)^2\rangle = 4(\langle {n_1}^2\rangle - \langle n_1\rangle^2) \qquad (38)$$

$\langle {n_1}^2\rangle$ and $\langle {n_2}^2\rangle$ can be evaluated reiterating the procedure of *"generating function"* used before[16]:

$$\langle {n_1}^2\rangle = \left[x\frac{\partial}{\partial x}\left(x\frac{\partial Z(x,y)}{\partial x}\right)\right]_{\substack{x=p\\Y=q}} \qquad (39)$$

$$\langle {n_1}^2\rangle = \left[y\frac{\partial}{\partial y}\left(y\frac{\partial Z(x,y)}{\partial y}\right)\right]_{\substack{x=p\\Y=q}} \qquad (40)$$

finding:

$$\langle {n_1}^2\rangle = (np)^2 + Npq = \langle n_1\rangle^2 + Npq \qquad (41)$$

The mean square displacement is[16]:

$$\langle(\Delta m)^2\rangle = 4Npq \qquad (42)$$

Taking the square root of equation (42), if p=q=1/2, as done in the previous case:

$$w = \sqrt{\langle(\Delta m)^2\rangle} = \sqrt{4Npq} = \sqrt{N} \qquad (43)$$

representing the fluctuation: the width of the range over which m is distributed after N steps.

If many particles diffusing in a viscous medium are considered, any trajectory is comparable with a random walk. The average displacement *m* covered by the ensemble of particle is zero. Taking into account only a

single particle the typical displacement m^*, from the origin of the path after N steps in one dimension, will be[16]:

$$\langle m \rangle - w \leq m^* \leq \langle m \rangle + w \qquad (44)$$

After N steps, separated by time windows τ (the time interval between two jumps, due to the collision of the particle with the chaotic motion of the solvent), the overall time will be $t = \tau N$ and the particle will diffuse with a coefficient of $D = {a_0}^2/\tau$. The typical displacement of particle as function of time will be[29]:

$$m^* \begin{cases} \sqrt{Dt} \\ Vt \end{cases} with \begin{vmatrix} p=q=\frac{1}{2} \\ p \neq q \quad ad \quad V=\frac{(p-q)}{a_0} \end{vmatrix} \qquad (45)$$

V is the drift velocity. The results obtained are in agreement with the observations made by Einstein and Fick: in fact the two equations give the same conclusion starting from different approaches. For very large values of N the binomial distribution can be approximated by a Gaussian distribution centred around the maximum $\overline{n_1}$, the mean value of the ensemble average. For large N the discrete variable n_1 becomes continuous and the sum is replaced by an integral, normalizing the probability and using the condition $\Delta n_1 = 1$[16]:

$$\sum_{n_1=0}^{N} n_1 P_N(n_1) = \sum_{n_1=0}^{\infty} n_1 P_N(n_1) \Delta n_1 \qquad (46)$$

for large N[16]:

$$\sum_{n_1=0}^{N} n_1 P_N(n_1) \Delta n_1 = P(\overline{n_1})\sqrt{N} \int_{-\infty}^{+\infty} e^{\frac{-x^2}{2pq}} dx = 1 \qquad (47)$$

with [16]:

$$P(\overline{n_1}) = \frac{1}{\sqrt{2\pi Npq}} \qquad (48)$$

The Gaussian distribution will be[16]:

$$\overline{P}_N(m) = \frac{1}{2} \cdot \frac{1}{\sqrt{2\pi Npq}}\, e^{\left[-\frac{1}{8Npq}(m-Np+Nq)^2\right]} \qquad (49)$$

Centred around the mean $\overline{m}$ [16]:

$$\overline{m} \begin{cases} 0 \\ N(p-q) \end{cases} with \begin{vmatrix} p=q=\frac{1}{2} \\ p\neq q \end{vmatrix} \qquad (50)$$

and the standard deviation[16]:

$$\langle (\Delta m)^2 \rangle = 4Npq \qquad (51)$$

1.6 DIGITAL VIDEO MICROSCOPY AND PARTICLE TRACKING.

Recent progress in analysis of optical microscope images is a new tool to study colloidal systems. in the '90s these methods underwent a rapid development, in particular in the quantitative studies of Brownian motion [18], phase transition [19-27], to probe the effects of external fields on the colloidal system[28] and pairs interactions between microspheres [29-31]. In particular, video microscopy is a powerful technique that allows to extract useful information in dynamic colloidal studies. Analysing the video image sequences recorded by microscopy is

possible to evaluate the spatial and temporal evolution of the system. Standard commercial cameras produce a video sequence at 30 frames per second (fps). A Scientific camera, such as Hamamatsu Orca flash 4.0, at full resolution of 2048 x 2048 pixel has a performance of 100 fps, but reducing the sensor scanning area it is possible to get to 1000 fps frame rate and more.

With a conventional optical microscope with a objective oil lens of 100x, the spatial xy resolution is of the order 65 nm per pixel.

Considering a colloidal suspension of latex particles with sub-micrometric dimension diffusing in a generic medium, it is possible to measure the trajectories evolution in time and evaluate several physical quantities (e.g. mean square displacement) by video analysis. The time evolution of the density operator distribution in the equation (1) can be used to calculate for an ensemble of N non interacting particles:

$$\rho(r,t) = \sum_{i=1}^{N} \delta\big(r - r_i(t)\big) \qquad (52)$$

The evolution of the density operator is intrinsically linked to other interesting physical quantities of interest and to analyse it requires specific software.

The software structure is built on five logical steps: the correction of image imperfections, locating of the particle positions, refining the positions, discriminating the “false” particles and linking the positions to obtain trajectories.

The first step consists in, subtracting off the background noise. The non uniform illumination of the pixels and the different sensitivity of each pixel generate a contrast gradient. If the particles are well separated the background noise is well modelled by a boxcar average function extended in a region of diameter $2w + 1$, with w integer larger

than particle radius but smaller than a sphere separations between a particle pair[32]:

$$A_w(x,y) = \frac{1}{(2w+1)^2}\sum_{i,j=-w}^{w} A(x+i, y+1) \qquad (53)$$

Digitization processes in the camera and in the frame grabber originates a random noise with correlation length $\lambda_n \simeq 1\, pixel$. The Gaussian surface of revolution is a good function to do a convolution and suppressing this noise[32]:

$$A_{\lambda_n}(x,y) = \frac{1}{B}\sum_{i,j=-w}^{w} A(x+i, y+j) e^{\left(\frac{i^2+j^2}{4\lambda_n^2}\right)} \qquad (54)$$

with:

$$B = \left[\sum_{i=-w}^{w} e^{\left(-\frac{i^2}{4\lambda_n^2}\right)}\right]^2 \qquad (55)$$

The "ideal" image can be expressed by the difference by the noise-reduced image and the background noise.

The second step in the analytical process consist in the particle location. In this step the aim is defining the pixel coordinate of the mass centroids of the particles. The criteria of the local brightest intensities is used to define the centroid: in practice the pixel is chosen as possible centroid if in the neighbourhood of it, there is not another pixel brighter. Once found the brightest pixel in the images, the requisite to be considered a centroid is that the intensity is located upper the 30th percentile of the brightness for the entire image[32].

The third step is the refining of the position of the centroid estimates in the second step[32] Moment distributions of the sphere brightness

images are calculated to distinguish noise from real spot. The objective is reducing the uncertainty of the centroid and reducing the standard deviation of the position in un a range of 1/10 pixel.

Afterward the position of the centroid are linked obtaining a set of trajectories. For a particle centroid, in one frame, the algorithm takes into account only the nearest particle in the subsequently frame to built a unique trajectories. This is possible only in dilute system. Choosing a value of max displacement between two subsequently frames, the more probable trajectories, in Brownian motion, is reached evaluating the probability (49). In this way is possible reducing the complexity of the problem and the linking procedure is easier to compute.[32]

With tracked data is possible to do an accurate analysis, calculating the MSD of the ensemble.

1.7 EXPERIMENTAL SETTING

The setting of the particle tracking technique was tested and calibrated trough several experiments in standard solutions at viscosity known and tabulated in the literature. As standards, pure water and several glycerol solutions at different concentrations were used. The colloids suspensions were obtained dispersing latex particles, labelled with a fluorescent green dye, of known diameters: 100 nm and 500 nm. From the analysis of the fitting of the mean square displacement, obtained by the video sequence analysis, was calculated the viscosity η through the Stock Einstein equation []. These data were compared with results present in literature and with rheological measurements, performed to find the η viscosities. The relation (24) is used to compare

the viscosities probed trough the particle tracking technique and the macroviscosity, found with rheological measurements.

1.8 MATERIALS AND METHODS

1.8.1 Glycerol suspensions:

Glycerol solutions in different concentrations were prepared. Glycerol (Sigma-Aldrich) was diluted in ultra pure milli-Q water at weight fractions: 10%, 30%, 50% w/w. The solutions were stirred for 1 hour. 10 μL of a stock of a green fluorescent latex suspension, 100 nm and 500 nm diameter, were added to the 1 mL of the glycerol solutions and dispersed, obtaining a final concentrations in volume <1%. The suspensions were sonicated for a 1 hours, avoiding the formation of aggregates.

1.8.2 Microscope, fast camera and video sequences:

The instrument used was a Olympus X81 inverted microscope with an Olympus 100x Uplsapo 1.4 numeric aperture objective. The illumination was a Hg lamp emitting a continuous spectra. A dichroic filter was used to select a opportune wave length of 480 nm in excitation and 520 nm in emission.

The samples, particle suspensions, in the chamber slides were loaded.

The image sequences were recorded with Hamamatsu Orca Flash 4.0. This camera is a CMOS technology and allows to record a stack image of a 512 x 2048 pixel at frame rate of 400 fps corresponding a time windows acquisition of 0.0025 s. The pixel size of this camera is 6.5 um

and this value, coupled at 100x optics, allows to obtain a pixel resolution of 0.065 micron/pixel.

For each concentrations were achieved 12 video sequences of 1000 frames length. All video sequences were sampled in different xy positions of the camber slide. The focus position was fixed at least to 10 μm up the bottom of the chamber, avoiding the hindrance effect of the slide floor, and for every single acquisition was used a different z height of focus.

With a k-thermocouple immersed in the chamber slides the temperatures were read.

1.8.3 Calibration data analysis:

The software used for a particle tracking is "Eclipse", a free licence IDL compiler. The script package, and relative tutorial, is available at web page of Harvard University[33].

In the tracking analysis a parameter of a minimum distance of separation, about 4 μm, between each particle couples was adopted: indeed frame with particles closer than this distance are neglected. Only a trajectories with at least 10 continuous jumps were selected, deleting shorter paths. The mean square displacements were extract from tracking and saved in a set of files for different concentrations of Glycerol solutions. These data were exported in text files and successively fitted with Origin 8.0 software. The mean square displacements were plotted as function of time. The points of mean square displacement for each time windows were fitted with a linear curves as reported in figures 1a and 1b .

1.9 CALIBRATION RESULTS AND DISCUSSION:

The time interval selected in the fitting data corresponds to a linear behaviour region, where a unit slope represents a diffusive regime. The deviation of the zero intercept in diffusive fitting is an estimate of error [34], arising in part from short rapid diffusion and in part from measurements errors which contribute $2d\Delta_{\epsilon}^{2}$.

The fitting plot are reported in figure 2 and figure 3. The diffusion coefficients, calculated trough the MSD are reported in Table 1 and Table 2. In figure 4 the viscosity values are reported as function of the shear rate, calculated with rheological measurements for three glycerol/water concentrations. All measurements are performed at 25 °C. In this condition, by knowing the viscosity values, is possible to compare the diffusion coefficients calculated with particle tracking technique with the diffusion coefficients obtained by theoretical values, applying the Stokes Einstein relation. In this Newtonian fluid there is good agreement between the two values, verifying that the viscosity probed by the particles, in the particle tracking technique, and the macro viscosity measured with the rheometer are very similar.

Glycerol %	$\boldsymbol{D\ [\mu m^2 s^{-1}]}$ **theoretical**	$\boldsymbol{D\ [\mu m^2 s^{-1}]}$ **particle tracking np 500 nm**	**Error Particle tracking**
0	0.98	0.96	0.01
10	0.73	0.77	0.01
30	0.38	0.37	0.02
50	0.16	0.17	0.004

Table 1 Theoretical and experimental diffusion coefficients for a beads of 500 nm diameter

Glycerol %	$D\ [\mu m^2 s^{-1}]$ theoretical	$D\ [\mu m^2 s^{-1}]$ particle tracking np 100 nm	Error Particle tracking
0	4.90	4.86	0.01
10	3.64	3.75	0.01
30	1.90	1.94	0.02
50	0.79	0.82	0.004

Table 2 Theoretical and experimental diffusion coefficients for a beads of 100 nm diameter

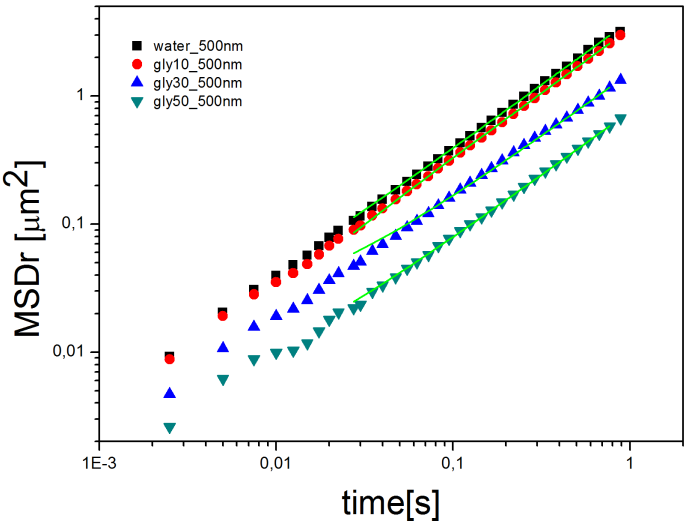

Figure 2: Fitting of the MSD for beads of 500 nm in different water/glycerol mixtures

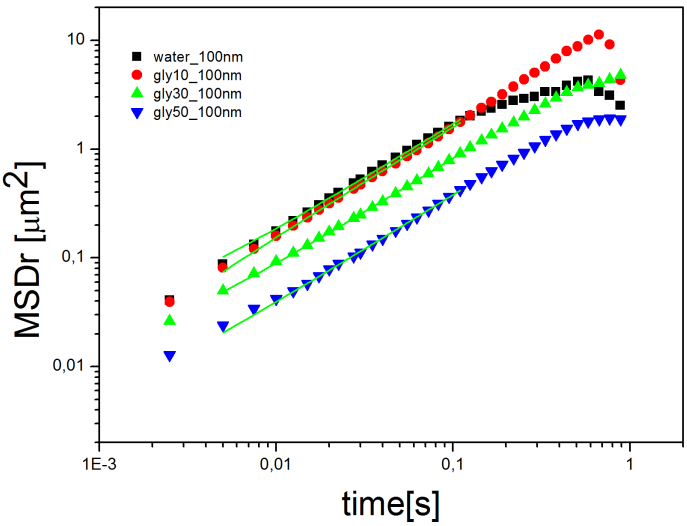

Figure 3: Fitting of the MSD for beads of 500 nm in different water/glycerol mixtures

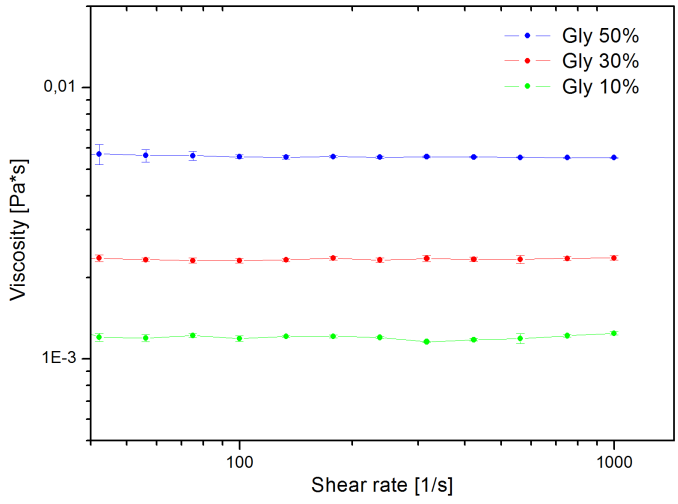

Figure 4: Rheological experiments for different Glycerol/water mixtures. The viscosity η in function of the shear rate.

2.10 CONCLUSION

In this chapter theoretical aspects of diffusion are explored by the classical and the statistical point of view.

Experiments analysing different standard solutions of Newtonian fluids with particle tracking technique are performed. These results are in agreement with rheological measurements and can be used to verify the correct calibration of the all parameters in particle tracking experiments.

References:

[1] Jean Philibert - Diffusion Fundamentals 2 (2005) 1.1 - 1.10

[2] Chaikin, P.M., Lubensky, T.C., Principle of condensate matter, Cambridge-(8-34)

[3] ibid page (369)

[4] ibid page (369)

[5] ibid page (369)

[6] ibid page (370)

[9] ibid page (370)

[8] ibid page (370)

[9] ibid page (370)

[10] ibid page (370)

[11] ibid page (371)

[12] ibid page (369)

[13] ibid page (373)

[14] ibid page (374)

[15] ibid page (374)

[16] Antonio Coniglio, Elementary course in statistical mechanics

[17] Reif, Fundamentals of Statistical and Thermal Physics, McGrow Hill

[18]Perrin,J.,"Atoms"(D.LI. Hammick, Trans.), Constable,London,1920]

[19] van Winkle, D. H., and Murray, C. A., Phys. Rev. A 34, 562 (1986)

[20] [Grier, D. G., and Murray, C. A., J. Chem. Phys. 100, 9088 (1994)

[21] Weiss, J. A., Oxtoby, D. W., Grier, D. G., and Murray, C. A., J. Chem. Phys. 103, 1180 (1995) .

[22] Pieranski, P., Strzlecki, L., and Pansu, B., Phys. Rev. Lett. 50, 900 (1983) ;

[23] Murray, C. A., and van Winkle, D. H., Phys. Rev. Lett. 58,(1987)

[24] Murray, C. A., Sprenger, W. O., and Wenk, R. A., Phys.
Rev. B 42, 688 (1990)

[25] Poulingy, B., Malzbender, R., Ryan, P., Clark, N. A., Phys. Rev. B 42, 988 (1990)

[26] Poulingy, B., Malzbender, R., Ryan, P., Clark, N. A., Phys. Rev. B 42, 988 (1990)

[27] Kusner, R. E., Mann, J. A., Kerins, J., and Dahm, A. J., Phys. Rev. Lett. 73, 3113 (1994)

[28] Skjeltorp, A. T., J. Magn. Mater. 65, 195 (1987) ; Okubo, T., J. Chem Soc., Faraday Trans. 1 84, 3377 (1988)

[29] Crocker, J. C., and Grier, D. G., Phys. Rev. Lett. 73, 352 (1994) .

[30] Kepler, G. M., and Fraden, S., Phys. Rev. Lett. 73, 356 (1994) .

[31] Vondermassen, K., Bongers, J., Mueller, A., and Versmold, H., Langmuir 10, 1351 (1994) .

[32] Crocker, J.C.,Grier, D. G., J. of Colloid and interface science 179, 298-310 (1996)

[33] http://weitzlab.seas.harvard.edu/ (last access 12/2013)

[34] Savin, T., Doyle, P., Biophysical Journal, 88-1, (2005)

CHAPTER 2: HINDERED BROWNIAN DIFFUSION IN SQUARE-SHAPED GEOMETRIES: THE DIHEDRAL EDGE EFFECT.

ABSTRACT

We studied the hindered diffusion generated by the edge effects due to a dihedral angle in a squared microtube. We measured the perpendicular D_y and parallel D_y components of the diffusion coefficient of a fluorescent latex 1 μm particle suspended in aqueous solution and loaded in a borosilicate squared capillary of 50 μm section side. Confocal Particle Tracking was used to measure the spatial dependence of the diffusion coefficient in a set of different planes, from the bottom of the capillary to a wide range up. The understanding of the spatial dependence of the diffusion coefficients in such a complex confined geometry of double perpendicular walls was achieved analysing the components of D_x and D_y as a function n of the distance from both channel walls, thus obtaining a set of curves parametrically dependent on the quote. Near the edge, the diffusion is hindered to a value of $\sim 0.4 D_0$ the unconfined diffusion, and the plateau regime is reached at a distance from the wall of 3 and 6 times the length of the particle diameter for D_x and D_y components respectively. The evidence of the edge effect in hindered diffusion phenomena is also examined in depth by simulation studies.

2.1 INTRODUCTION

Diffusion in confined environments as cavities, tubes, porous systems is relevant in several applications, e.g. biological processes where nanovectors functionalized with specific molecules diffuse in complex structures, entrapment of particles in microporous materials, controlled-diffusion reaction mechanisms, coating processes or other applications involving microfluidic chips [1-3] and surface-based biosensor [4]. Understanding the diffusion mechanism in three-dimensional confined environments could improve the engineering of diffusion-limited processes in relevant systems such as interfaces and near cell lipid membranes, thus highlighting the relevance of confined diffusion also in bioscience[5].

Several simplified models have been developed in simple geometries useful to understand the diffusion in confined systems [6-10]

The problem of diffusion of colloidal spherical particles near a single flat wall was mathematically solved by Lorentz[11] and Faxen[12][13] through the numerical solution of Navier-Stokes equations. Later, the solution was improved by Brenner[14] and extended to the double-wall case by Goldman[15]. Oseen introduced the two parallel infinite walls model, where the effect of the double confinement was considered additive [16]. Analytical predictions in more complex geometries, however, cannot be easily performed.

With the introduction of new experimental techniques as dynamic-light-scattering [17], video microscopy [18-19], digital imaging[20], and the controlled manipulation of colloidal spheres through optical tweezers [21-22], new evidences of the wall effects on the diffusion coefficients have been reported. Lin et al , by combining video

microscopy and optical tweezers, analysed the effect of a single flat wall on the diffusion of s spherical particle [18]. The influence of two parallel plates was experimentally investigated by Dufresne et al. They found a good agreement between the measured diffusion coefficients and those calculated from the drag predictions for the two infinite parallel plates case [19]

Recently, the effect of a closed cylinder cavity on the diffusivity was studied. The axial, radial and azimuthal components of the diffusion tensor were measured [23] and computed by hydrodynamic numerical simulations [24]

In the fabrication of the microfluidic channels, through the milling process, are almost obtained a square channel sections. These fabrication are used in a wide field of applications and it's useful understanding the diffusion properties of colloids in proximity of the edges.

In this work, we investigate the diffusion behaviour of particles in a square-shaped capillary. In particular, we focus on the effect on the diffusion coefficients of two orthogonal walls (near the channel edge). Digital video microscopy [25] combined with confocal microscopy allowed the accurate measurement of diffusion coefficients from the particle trajectories along two perpendicular directions of the channel section. Finite element simulations are performed to support the experimental results.

2.2 HINDERED BROWNIAN MOTION OF ISOLATED SPHERES NEAR A WALL

A hard latex sphere of radius $a = \mathbf{d}/2$ immersed in a Newtonian fluid of viscosity η and speed $\boldsymbol{u}$, is subject to a drag resistance opposed to the direction of motion. Under no slip boundary conditions and for low Reynolds numbers of the fluid, the drag force can be expressed by the Stokes Law

$$F_0 = -6\pi a\boldsymbol{u} \qquad (1)$$

While the Stokes Einstein relation gives the value of the coefficient of diffusion

$$D_0 = \frac{K_b T}{6\pi\eta a} \qquad (2)$$

at fixed temperature T and with K_b equal to Boltzmann constant.

If the particle is close enough to the wall, the influence of the wall is appreciable, hindering particle movements. Separating the two linear components of the motion, parallel and perpendicular with respect to the wall, a new expression can be written taking into account the product of not hindered diffusion coefficient multiplied for a correction factor λ

$$D_{\parallel} = \frac{K_b T}{6\pi\eta\lambda_{\parallel} a} = {\lambda_{\parallel}}^{-1} D_0 \qquad (2a)$$

$$D_{\perp} = \frac{K_b T}{6\pi\eta\lambda_{\perp} a} = {\lambda_{\perp}}^{-1} D_0 \qquad (2b)$$

Usually an analytic closed solution for the diffusion coefficient accounting for the wall effect in low Reynolds numbers is not available. Most of the times an approximate solution is used. The $\lambda_{\perp}$ coefficient, of the perpendicular component, was calculated by Brenner , according the following equation[18]:

$$\lambda_{\perp}^{-1} = \frac{D_{\perp}}{D_0} = \left\{\frac{4}{3}\sinh\alpha \sum_{n=1}^{\infty} \frac{n(n+1)}{(2n-1)(2n+3)} \left[\frac{2\sinh(n+1)\alpha + (2n+1)\sinh\alpha}{4\sinh^2(n+1/2)\alpha - (2n+1)^2\sinh^2 2\alpha}\right]\right\}^{-1} \quad (3)$$

where $\alpha = \cos^{-1}(y_s/\mathrm{a})$ and y_s is the position of the beads with respect to the wall.

Another method of calculating the λ coefficients is the so called *"Reflection method"*, in which a series expansion can help to explain the effect of the wall on the diffusivity. This due to the variation of pressure and velocity distributions induced by the sphere in the surrounding fluid when the particle is near a wall. The expansion is usually truncated to the first term, as equations 4a and 4b show:

$$\lambda_{\parallel}^{-1} = \frac{D_{\parallel}}{D_0} \cong 1 - \frac{9}{16}\left(\frac{a}{y_i}\right) + O\left(\frac{a}{y_i}\right)^3 \quad (4a)$$

and

$$\lambda_{\perp}^{-1} = \frac{D_{\perp}}{D_0} \cong 1 - \frac{9}{8}\left(\frac{a}{y_i}\right) + O\left(\frac{a}{y_i}\right)^3 \quad (4b)$$

In the case of a sphere situated at an arbitrary point between two parallel walls, the method of reflections doesn't give an accurate solution, except for the limit case of a particle situated in the middle plane between two parallel walls.

Alternatively the Oseen [25] solution is based on the idea that the hindrance effect of double parallel walls could be additive, deriving the following equation for the parallel component [18]:

$$\frac{D_{\parallel}}{D_0} \cong 1 - \frac{9a}{16}\left(\frac{1}{y_i} + \frac{1}{\mathbf{L}_y - y_i}\right) \qquad (6a)$$

this equation can be also adopted for the perpendicular one:

$$\frac{D_{\perp}}{D_0} \cong 1 - \frac{9a}{8}\left(\frac{1}{y_i} + \frac{1}{\mathbf{L}_y - y_i}\right) \qquad (6b)$$

These equations are first order approximations, where the high order of the sum are neglected.

2.3. PROBLEM FORMULATION:

Aim of this work is to investigate the hindered diffusion of a Brownian particle inside a square cavity. In figure 1, a schematic representation of the geometry is shown. A particle with radius $a = \mathbf{d}/2$ is immersed in a Newtonian fluid that fills a channel with a square cross-section. A Cartesian reference frame is considered with origin at one corner of the channel cross section, in the middle position between the two extremities, with x the direction of the channel axis, and y and z the directions parallel to the channel lateral walls (see figure 1). We denote

with L_x, $L_y$and L_z the channel sizes along the $x-$, $y-$ and $z-$direction. The length L_x, is selected much larger than the other two in order to neglect any effect due to the two channel extremities. In this way, the $x-$position of the particle x_p is irrelevant, provided that it is located in a region sufficiently far from the channel extremities. The $x-$ and $z-$positions are denoted by y_p and z_p, respectively. Because of the Brownian motion, the particle randomly moves in the fluid. The presence of confining walls are expected to modify the diffusion with respect to the bulk behaviour. We are interested in measuring the diffusion coefficients along the $x-$ and $z-$directions, denoted by D_x and D_y respectively. Both diffusion coefficients depend on the position of the particle in the channel cross-section. It is convenient to express the diffusion coefficients as a function of the distance from the closest walls $D_x(y_d, z_d)$ and $D_y(y_d, z_d)$ (figure 1). Notice that the distances are computed from the particle centre, i.e. $y_d = a$ or $z_d = a$ means that the particle touches one of the walls. Finally, we remark that, because of the symmetry, the diffusivities along y and z are related by the following relation $D_y(y_d, z_d) = D_z(z_d, y_d)$. Furthermore, for the same reason the translational diffusion tensor $\boldsymbol{D}$ is diagonal. Therefore, the knowledge of D_x and $D_y$is sufficient to completely describe the translational diffusion behaviour.

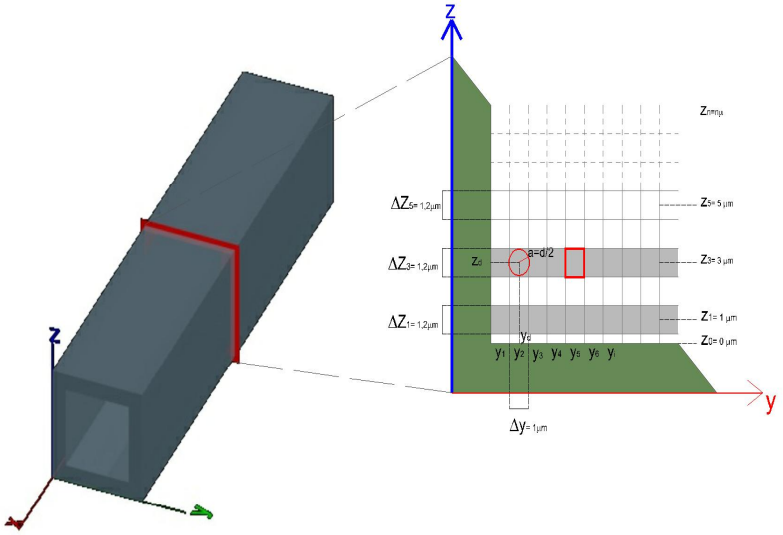

Figure 1: Volume partitioning: 3D representation of square tubing geometry with left handed coordinate system. In the inset the cross section is represented. with Δy section of 1 µm on the y axis at y_i distance from the xz lateral wall and Δz confocal section of 1.2 µm on the z axis at z_i .distance. The red circle is the polystyrene particle of d=1.1 µm.

2.4.1 NUMERICAL SIMULATIONS:

The prediction of the diffusion coefficients D_x and D_y is carried out by numerical simulations. A single, rigid, spherical particle immersed in a Newtonian, inertialess fluid that fills a channel with a square cross-section is considered. The equations governing the fluid motion are the mass and momentum balance equations:

$$\nabla \cdot \boldsymbol{v} = 0 \qquad (7a)$$

$$\nabla \cdot \boldsymbol{\sigma} = \mathbf{0} \qquad (7b)$$

where $\boldsymbol{v}$ is the fluid velocity and σ is the stress tensor expressed as $\boldsymbol{\sigma} = -p\boldsymbol{I} + 2\eta\boldsymbol{D}$, with p the pressure, $\boldsymbol{I}$ the identity tensor, η the fluid viscosity and $\boldsymbol{D} = (\nabla\boldsymbol{u} + \nabla\boldsymbol{u}^T)/\boldsymbol{2}$ the rate-of-deformation tensor. On the domain boundaries, no-slip conditions are imposed. On the spherical surface, a velocity v_x or v_y is applied. After the solution, the force on the sphere (F_x or F_y) can be calculated and the hydrodynamic drags along the $x-$ and $y-$directions are given by:

$$\zeta_x = \frac{F_x}{v_x} \qquad (8a)$$

$$\zeta_y = \frac{F_y}{v_y} \qquad (8b)$$

By applying a generalized Stokes-Einstein relationship:

$$D_x = \frac{K_b T}{\zeta_x} \qquad (9a)$$

$$D_y = \frac{K_b T}{\zeta_y} \qquad (9b)$$

the diffusion coefficients are calculated.

The governing equations are solved by the finite element method. Concerning the computational domain, a parallelepiped with a square cross-section is chosen. With reference to figure 1, the length of the cross-section sides L_y and L_z, and the particle radius are selected so as to reproduce the experimental materials. The domain along x is chosen sufficiently long to assure unperturbed conditions along such a direction, i.e. an infinitely long channel is considered and the particle motion is only affected by the four lateral walls.

Simulations are performed by setting the sphere at different distances from the lateral channel walls, selected over a regular grid. The simulation data are, then, interpolated by using polynomial functions. In this way, the diffusion coefficients $D_x(y_p, z_p)$ and $D_y(y_p, z_p)$ are available over the whole channel cross-section.

2.5 MATERIALS

Polystyrene particles with $1.1 \pm 0.1\,\mu m$ diameter (Invitrogen), carboxylated on the surface and containing a red fluorescent dye (580/600 nm) were used. Stock dispersion 2% in weight of particles was sonicated for a few minutes to prevent aggregation, than was dispersed in 1:1 solution of MilliQ Ultrapure Water/Deuterium Oxide, obtaining a final volume fraction lower than 1%. This concentration corresponds to a $\sim 3.5 \cdot 10^{11}$ particles/ml. Sodium Chloride NaCl (Baker Analysed Grade) is added to the dispersion achieving a final concentration of $10^{-4} \div 10^{-3}$ mol/kg, corresponding to a Debye Screening Length about $10 \div 30$ nm; this value is enough to neglect the interparticle and particle-wall electrostatic repulsion. A Water/Deuterium Oxide solution matching the polystyrene microbeads density is suitable to prevent particle sedimentation.

The suspension was injected inside a square-shaped borosilicate capillary with an internal side of L_y = L_z = 50 mm (Vitrocom) and length $L_y$approximately 7 cm by a pressure pump to avoid partial filling of the internal volume and formation of air bubbles. Each extremity was sealed by a Bunsen flame. The capillary was laid down with the bottom wall

facing a coverslip glass of 0.17 mm thickness. The coverslip was surrounded with immersion oil ($n_e = 1.518$) to reduce the refractive index mismatch with the capillary glass. All experiments were performed at 295 K in thermostatic conditions.

2.6 METHODS

2.6.1 Confocal Scanning Laser Microscopy:

The analysis of the Brownian motion of particles within the channel was performed by particle tracking technique. The observation direction was from the bottom of the channel, i.e. from the z-axis (see figure 1). Therefore, to identify the $z-$position of the tracked particles, a Leica Sted SP5-CW confocal microscope with a wide set of different wavelength lasers and a 100x plan-apo 1.4 oil objective was used to acquire the image sequences. The height along the $z-$direction was measured through a galvanometric stage which allows focusing in z at 10 nm resolution. The reference of the bottom wall of the capillary was taken where the laser reflection intensity was maximum (figure 2a) In this position the confocal section thickness, measuring about 1.2 μm, is contained for one-half inside the thickness of the capillary glass wall and one-half in the sample. Particles were excited with a laser wavelength of 580 nm at 30% intensity, and the emission was collected between 600-650 nm with a PMT gain factor of 700 Volts. The video sequences were captured using the detector in resonant scanner mode in order to have a faster reading of pixel rows (8000 Hz), with sampling interval of Dt = 0.049 s, corresponding to a frame rate of 20.4 fps. The resolution used was 1024x660 pixel. The zoom factor was set to 2.70 X, obtaining a ratio

of 11.22 $pixel/\mu m$. The Figure 2b is an images of the particle moving in confocal the confocal slab.

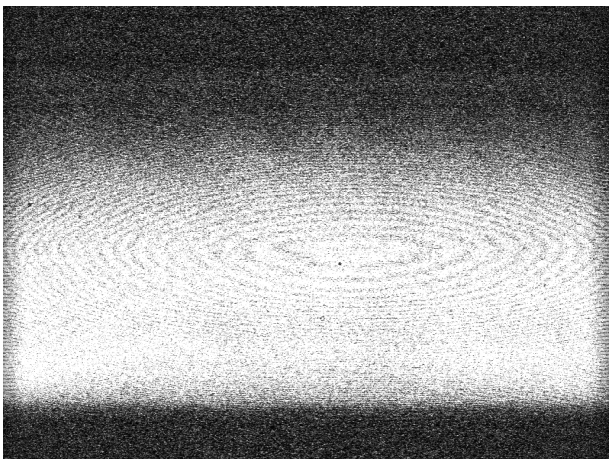

Figure 2a: Diffraction pattern generated from confocal laser reflection by the bottom capillary.

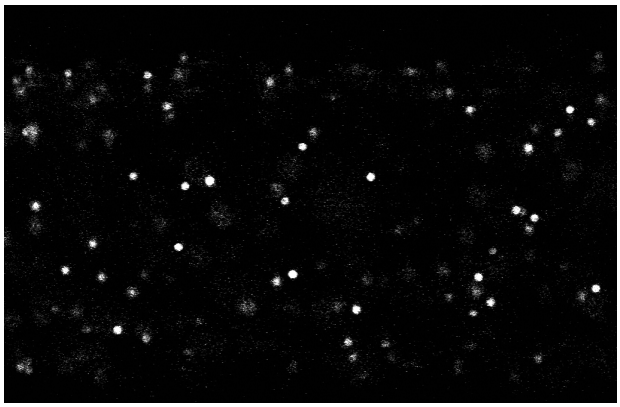

Figure 2b: Fluorescent yellow-green 1.1 μm polystyrene spheres in the z_2 confocal slab 1.2 μm thick at distance 1 μm from the bottom of capillary.

2.6.2 Channel section partitioning:

In confined systems, an issue concerning the attribution of the measured diffusivities to a specific point of the space arises. Indeed, as the diffusion coefficients are space-dependent and they are calculated from the particle trajectories, a criterion to assign the measured diffusivities to a point of the space is required. In this work, we partitioned the channel cross section in n_z −slabs along the z −direction, as shown in the inset of figure 1. The slabs corresponding to different heights of the confocal section were numbered starting from the bottom of the glass capillary. The width of each slab was $\Delta z = 1.2\,\mu m$, corresponding to the width of the confocal section (height of the Point Spread Function of the optical system). The distance between the midlines of two consecutive slabs was chosen as $1\,\mu m$. A description of the slabs is reported in Table 1. Every slab was, then, divided in n_y stripes along the y −direction, numbered starting from the left vertical wall. The width of the stripes was $\Delta y = 1\,\mu m$ and the distance between the midlines of consecutive stripes was $1\,\mu m$. Therefore, the channel cross-section is partitioned in a grid consisting of $n_y \times n_z$ elements. Each element is the cross-section of a box with length L_x (figure 3). The boxes are identified by the y and z coordinates of the center of the cross-section intervals. Each trajectory starting in a specific box contributes to the measurement of the diffusion coefficient (through the Mean Square Displacement (MSD), see below) assigned to that box. In this regard, we mention that previous investigations [24] showed that the MSD evaluation is essentially independent of the position attributed to the path (at the initial point, midway or the ending point).

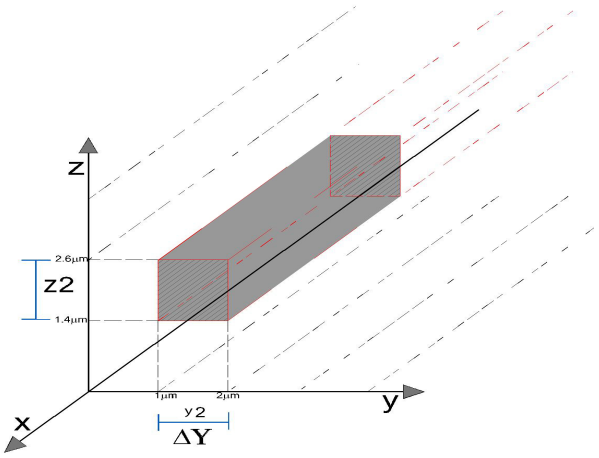

Figure 3: The dihedral edge is represented by two green planes. Particular of a box originated from the $z_2$slab at y_2 stripe. This discretization of the whole volume is operated for all y_i stripes at every z_n plane.

Slab	Thickness	Bottom-Top	Position
z_1	1.2 μm	0.4-1.6 μm	1 μm
z_2	1.2 μm	1.4-2.6 μm	2 μm
z_3	1.2 μm	2.4-3.6 μm	3 μm
z_4	1.2 μm	3.4-4.6 μm	4 μm
z_5	1.2 μm	4.4-5.6 μm	5 μm
z_6	1.2 μm	5.4-6-6 μm	6 μm
z_7	1.2 μm	6.4-7.6 μm	10 μm
z_{10}	1.2 μm	9.4-10.6 μm	10 μm

Table 1: the z_n confocal slabs. In this table the centre positions and the top and bottom extremes of the slabs are reported.

2.6.3 Image acquisition and processing:

For each slab along z, 30 video sequences were acquired up to n_z= 10. A single sequence is composed of 1500 frames, for about 40 minutes recording in each slab. When the acquisition of each video sequence is finished, the procedure of finding the bottom plane of the capillary is repeated and a snapshot is acquired as a reference. This operation limits the defocusing problem.

The video sequence was processed with ImageJ software to convert the raw data in 8bit image files. The routines available on Harvard University web site are used for particle tracking.[26] These routines have been modified in order to improve the quality of tracking excluding a too high spot intensity thus avoiding recording of aggregate particles. The average number of particles recorded in each plane was around one-hundred, which means that the free volume around a single particle is $\sim 110\ \mu m^3$, and the average separation distance between two particles is larger than $\sim 3.8\ \mu m$. A threshold distance is set in pre-tracking algorithms to neglect particles having centroids closer than $\sim 4.5\ \mu m$. Selected particles were restricted only to completely focused fluorescent objects through software evaluation of brightness and eccentricity, in order to further reduce the confocal section thickness. In each slab we tracked, on the average, a total number of $\sim 10^6$ particle jumps that is enough to obtain a good statistic.

2.6.4 Calculation of diffusion coefficients:

The matrices generated by the particle tracking software were processed in *Matlab*. The Mean Square Displacement (MSD) along the x and y axes has been evaluated as:

$$\langle \Delta x^2(\tau) \rangle = \langle [x(t+\tau) - x(t)]^2 \rangle \qquad (10a)$$

$$\langle \Delta y^2(\tau) \rangle = \langle [y(t+\tau) - y(t)]^2 \rangle \qquad (10b)$$

The average $\langle \dots \rangle$ is taken over all the times t and all the tracked particles. The MSDs are calculated for $\tau = \Delta t,\ 2\Delta t,\ 3\Delta t$ and $4\Delta t$, with Δt the aforementioned sampling time interval. Finally, the MSDs data are linearly fitted and the diffusion coefficients are calculated as:

$$D_x = \langle \Delta x^2(\tau) \rangle / 2\tau \qquad (11a)$$

$$D_y = \langle \Delta y^2(\tau) \rangle / 2\tau \qquad (11b)$$

The diffusion coefficients were evaluated independently in each stripe. We point out that, even for the largest τ considered in this work, the mean free path, estimated from unconfined conditions to be 200 nm, is much lower than the stripe width. Therefore a particle essentially tends to remain in the stripe it starts from. (figure 4).

The differences arising in the diffusion coefficients computed at different time windows were investigated by comparing the fitting slopes at times of $2\Delta t$, $3\Delta t$, $4\Delta t$. As reported in Figure 5, slopes are statistically similar, showing a linear behaviour with negligible deviations from linearity.

The analysis performed concerns the whole capillary volume, as evident observing the trajectories plot in figure 6; in particular the trajectories density increases from the bottom slab z_1 to the top one z_9.

Figure 7 reports representative jumps distributions recorded at 1, 2 and 3 μm distances from the *xz* wall at three different heights of 1, 3, 6 μm from the bottom wall. The distributions have all a symmetric Gaussian shape, typical of Brownian motion, where the probability of

making a jump in any direction is the same despite the wall presence. In particular, small lateral tails characterized by jumps larger than $\Delta y/2$ appear in jump distributions measured at y_1. This effect is more relevant moving to distributions at higher z_n planes, where the friction coefficient due to the effect of the bottom xy plane hindering particles displacements is less detectable. Indeed, jumps are here hindered more by the lateral xz wall presence. Though evidences of these rare events are recorded in the distributions shown, the assignment of 1 μm width in the lateral discretization procedure maintains the Gaussian shape of the overall distributions measured.

As a side note, we mention that the same procedure has been used to evaluate the mean mixed term displacement $\langle \Delta x \Delta y \rangle$. As expected, such a term is very small compared to the MSDs in x and y ($\sim 10^{-5} \div 10^{-4}$).

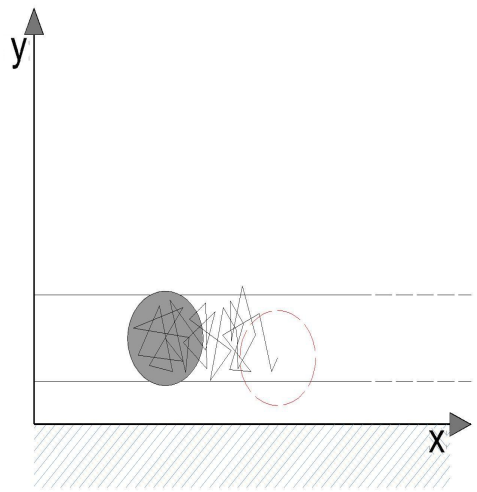

Figure 4: xy projection: observer view. Representative trajectory of a particle that does not escape the $y_i$discretized section in the time window analysed.

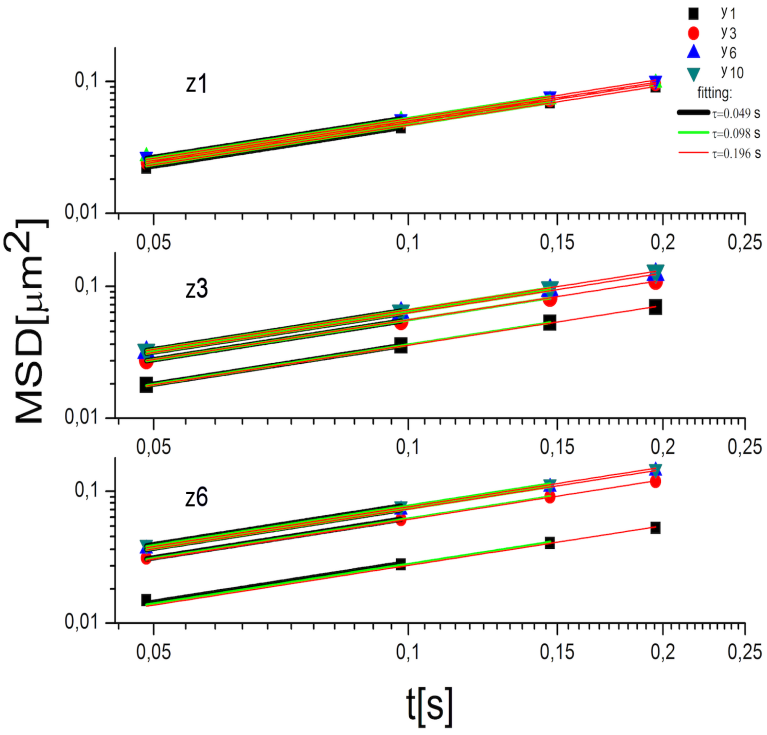

Figure 5 Linear fitting for slabs z_1, z_3 and z_6 at $\tau = 2\Delta t$, $\tau = 3\Delta t$ and $\tau = 4\Delta t$. The linear fitting shows no dependence by the time window length

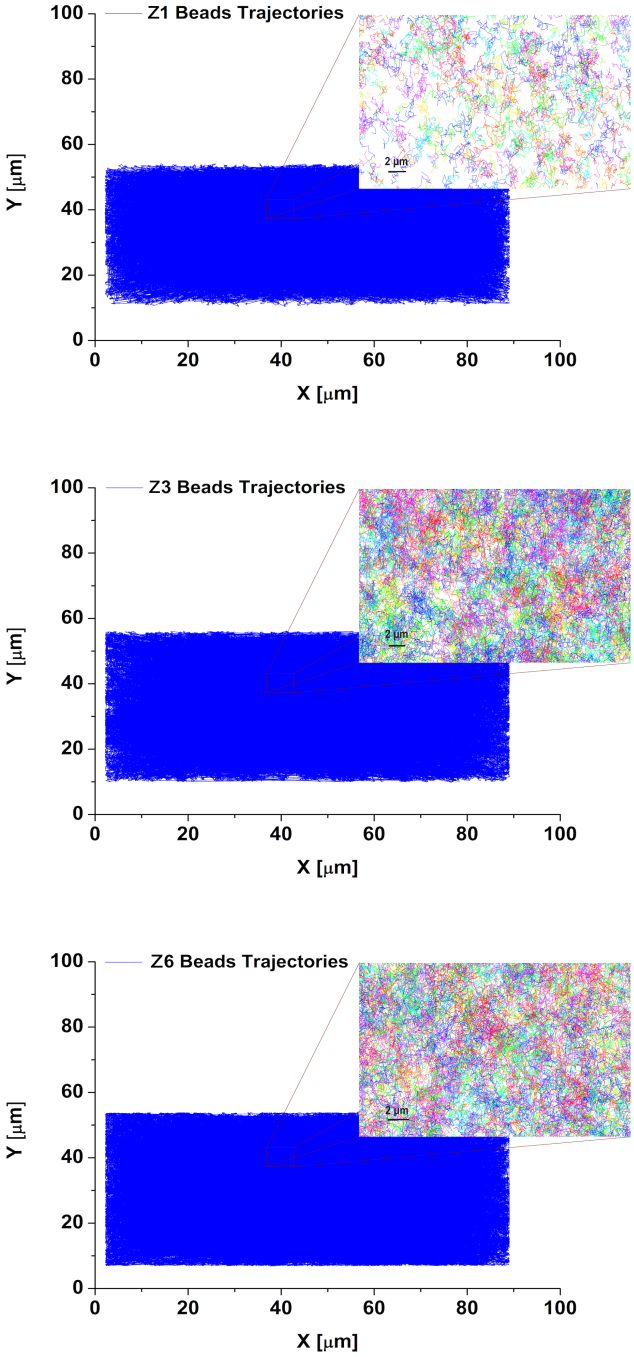

Figure 6: Beads trajectories. Trajectories densities are shown in blue in each slab. Insets show portions of capillary with differently colored bead trajectories. z_0 shows a density lower than the other slabs.

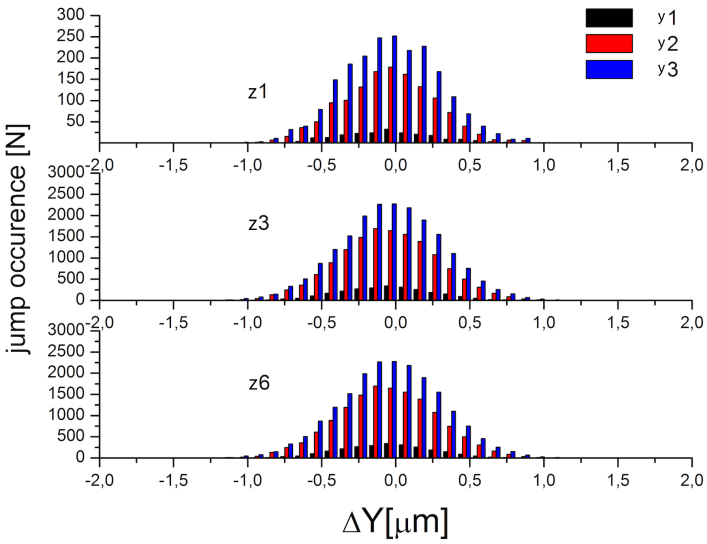

Figure 7: Different stripes centred at distance of 1, 2 and 3 μm with respect to the xz wall (y_1, y_2 and y_3 shown in black, red and blue respectively. The Jump length statistical distribution in y direction measured at 4τ. Gaussian shapes confirm Brownian regime. Mean free path length is shorter than the Δy width.

2.7 RESULTS AND DISCUSSION

The displacements of Brownian particles diffusing close to a dihedral edge of a square section capillary were measured and their space dependence was investigated along the x and y axes independently, obtaining the two components D_x, D_y.

Both diffusion coefficient respect to the lateral xz channel wall, D_x and D_y respectively, were computed. These data were grouped as a function of the normalized distances $\Lambda = \frac{y_i}{\mathrm{d}}$, thus obtaining a set of y_i curves for the z_n slabs evaluated. The components of the diffusion coefficient $D_x$and $D_y$were normalized to the values D_0, calculated in the middle of the microfluidic channel at z_9 in the central stripes y_i with i= 20 ÷ 30. The

values of D_x/D_0 and D_y/D_0 increase by increasing Λ and z_n, that is further from lateral and bottom confining walls. Both components, $D_x/D_0$and D_x/D_0, show higher variations in proximity of small values of Λ. In particular, the variation of the D_y/D_0 component is twice larger than that of the D_x/D_0 one, reaching is higher value as close as at 3Λ. In Figure 8b trends for the D_y/D_0 components show that it is hindered at distances up to 6Λ, while reaching unity smoothly in the middle of the channel.

These behaviours are similar for each curve computed in different z_n slabs. All z_n curves are distinguishable; in particular for higher z_n, curves attain higher values closer to the lateral wall than at lower slabs, which is due to the reduction in residual hindrance exerted by the bottom wall.

A greater uncertainty is associated to the diffusion coefficients computed close to the lateral wall at y_1, due to lower particle occupancy in its proximity.

The total amount of $\sim 10^6$ particle positions observed in each slab is theoretically distributed in time among the y_i stripes, thus, an average mean density of the order $2 \cdot 10^4$ for each stripe is expected. Interestingly, we measured the occurrence of the particle occupancy with deviations from homogeneity of the order $\sim 98\%$ close to the walls, at y_1 in the z_1 slab, and of 94% at y_1 in the z_3 slab, which characterizes a depletion region that extends up to $3\ \mu m$ away from the lateral wall (Figure 9).

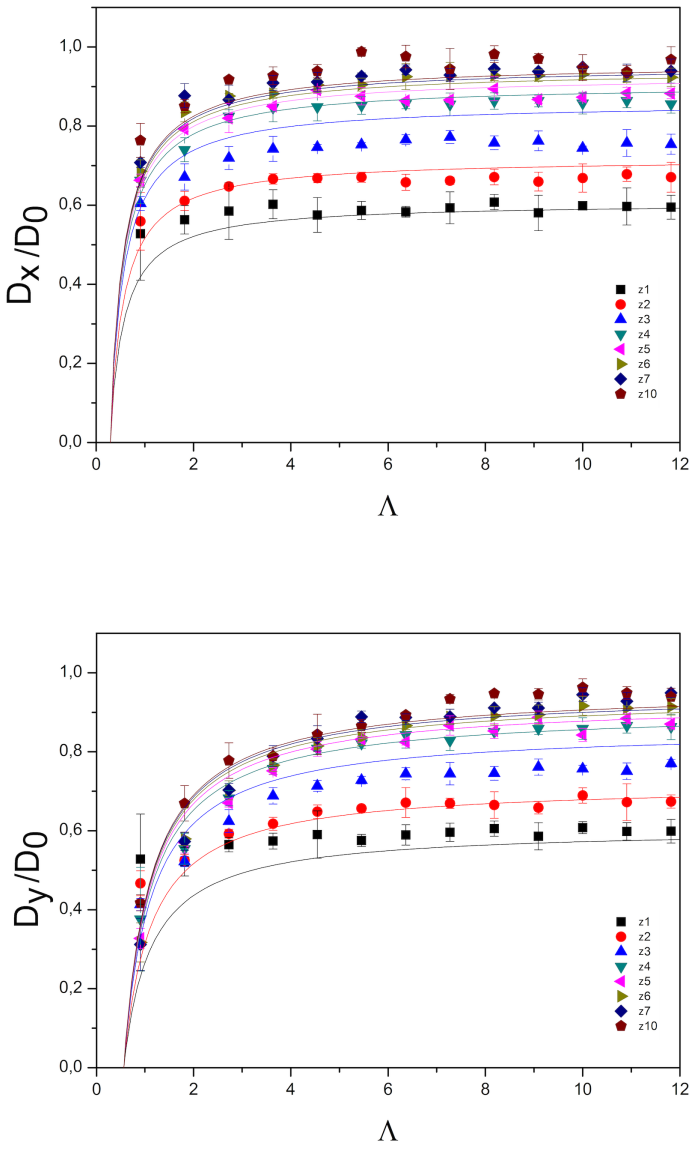

Figures 8a and 8b: Normalized Diffusion coefficients components as a function of normalized lateral confinement Λ. a) D_{xx}/D_0, b) D_{yy}/D_0. Each curve refers to a different z_n position. Only at large Λ the bulk value is asymptotically reached. Continuous lines are simulation analyses.

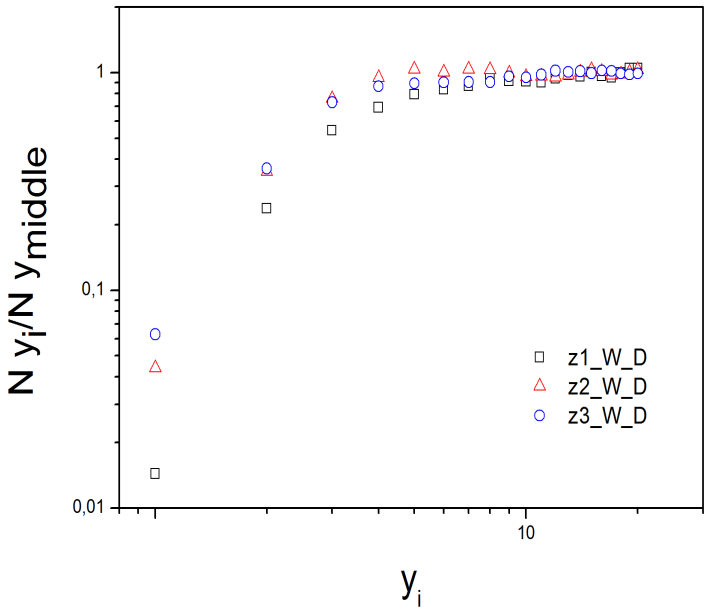

Figure 9: Statistical occupancy of each stripe for different z_9 slabs. Each slab occupancy is normalized for the occupancy value in the middle of the channel. A depletion region is observable close to the wall..

2.8 CONCLUSION

The displacements of Brownian particles of 1 um diffusing in a square cross section capillary of 50um side were measured by particle tracking technique in confocal fluorescence microscopy and their space dependence was investigated along the x and y axes independently, obtaining the two components D_x, D_y.

The values of the two components increase by increasing the distance z_n from the bottom wall and from y_n lateral wall. Both components show higher variations in proximity of the wall region. In particular, the

variation of the D_y component is twice larger than D_x. These results are in agreements with simulations. Interestingly, near the lateral wall a depletion region is observed. This region is about 3 times the size of the particle.

REFERENCES

[1] K. van Ommering, C. C. H. Lamers, J. H. Nieuwenhuis, C. L. J. van Ijzendoorn, and M. W.J. Prins, J. Appl. Phys. 105, 104905 (2009).

[2]K. van Ommering, J. H. Nieuwenhuis, C. L. J. van Ijzendoorn, L. J. Koopmans, and M. W. J. Prins, Appl. Phys. Lett. 89, 142511 (2006).

[3] Kim, S.; Seppo, S. J. Microhydrodynamics; Dover Publications: New York, 2005

[4]T. M. Squires, R. J. Messinger, and S. R. Manalis, Nat. Biotechnol. 26, 417 (2008).

[5]Zhang, Wei; Chen, Song; Li, Na; et al, Plos One,9,1,2014

[6] J. Happel and H. Brenner, Low Reynolds Number Hydrodynamics, Prentice-Hall International Series in the Physical and Chemical Engineering Sciences (1996).

[7] S. Kim and S. J. Karrila, Microhydrodynamics: Principles and Selected Applications (Butterworth-Heinemann, Boston, 1991).

[8]A. J. Goldman, R. G. Cox, and H. Brenner, Chem. Eng. Sci. 22, 637 (1967).

[9] A. Falade and H. Brenner, J. Fluid Mech. 193, 533 (1988).

[10] B. R. Hirschfeld, H. Brenner, and A. Falade, PCH, PhysicoChem. Hydrodyn. **5**, 99 (1985).

[12] Faxen, H. The resistance against the movement of a rigour sphere in viscous fluids, which is embedded between two parallel layered barriers. Ann. Phys. 1922, 4 (10), 79-89

[13] Faxen, H. Fredholm integral equations of hydrodynamics of liquids I. Ark. Mat., Astron. Fys. 1924, 18 (3), 29-32.

[14] Brenner, H. The slow motion of a sphere through a viscous fluid towards a plane surface. Chem. Eng. Sci. 1961, 16 (19), 242-251.

[15] Goldman, A. J.; Cox, R. G.; Brenner, H. Slow viscous motion of a sphere parallel to a plane wall**;** I. Motion through a quiescent fluid. Chem. Eng. Sci. 1967, 22 (14), 637-651.

[16] Oseen C. W., Neuere Methoden und Ergebnisse in der Hydrodynamik (Akademische Verlagsgesellschaft,Leipzig) 1927.

[17] L. Lobry and N. Ostrowsky, Phys. Rev. B 53, 12 050 ~1996**.**

[18] B. Lin, J. Yu, and S. A. Rice, Phys. Rev. E 62, 3909 **(**2000**).**

[19] E. R. Dufresne, D. Altman, and D. G. Grier, Europhys. Lett. 53, 264 **(**2001).

[20]L. P. Faucheux and A. J. Libchaber, Phys. Rev. E 49, 5158 **(**1994).

[21] A. Ashkin, J. M. Dziedzic, J. E. Bjorkholm, and S. Chu, Opt.Lett. 11, 288 **(**1986**)**.

[22] D. G. Grier, Curr. Opin. Colloid Interface Sci. **2**, 264 **(**1997**).**

[23] H. B. Eral, J. M. Oh, D. van den Ende, F. Mugele, and M. H. G. Duits, Langmuir 26, 16722 (2010).

[24] Imperio, A., Padding, J.T., Briels, W., J. Chem. Phys. 134, 154904 (2011);

[24]J. C. Crocker and D.G. Grier, journal of colloid and interface science 179, 298–310 (1996)

[25]Benesch, T,Yiacoumi, S, PHYSICAL REVIEW E 68, 021401 **(**2003)

[26] www.weitzlab.seas.harvard.edu (last access in 12/2013)

ABSTRACT

The diffusion problem of polyelectrolytes in a wide range of concentrations is here addressed The diffusive behaviour of particles in the dilute, semidilute and entangled regime are explored in terms of local properties related to the nanoviscosiy and macroscopic properties. The diffusion behaviour of nano particles of spherical shape and ellipsoid dispersed in different solutions of Hyaluronic acid is characterized. The diffusion coefficients of ellipsoids, at different stretching ratio are compared with the diffusivities of spherical particles. The values of nanoviscosity obtained by the particle tracking technique have been compared with the macroviscosity obtained from the Ubbelohde viscometer, obtaining information about the local properties and the caging effect of the mesh. The "shape" effect in particle diffusion in complex fluids is then evaluated.

3.1 INTRODUCTION

Polyelectrolytes solutions are an interesting class of polymers which are widely used in biomedical and industrial applications in different new technologies: drug delivery, soft tissues intensification to flocculation process[1]. Among the natural polyelectrolytes, hyaluronic acid (HA) is one of the most widely characterized since it has a fundamental role in human tissue, this is due to the relevant presence in the vertebrates tissues.

The knowledge of microscopic behaviour of this macromolecule structure and the diffusion properties a nano particle inside the interstitial environment generated by the polymer mesh, are very suggestive topics.

Hyaluronic Acid is a linear glycosaminoglycan consisting of repeating disaccharide units of N-acetyl-β-D-glucoronic acid alternately linked at the 1,3 and 1,4 positions, respectively[2].

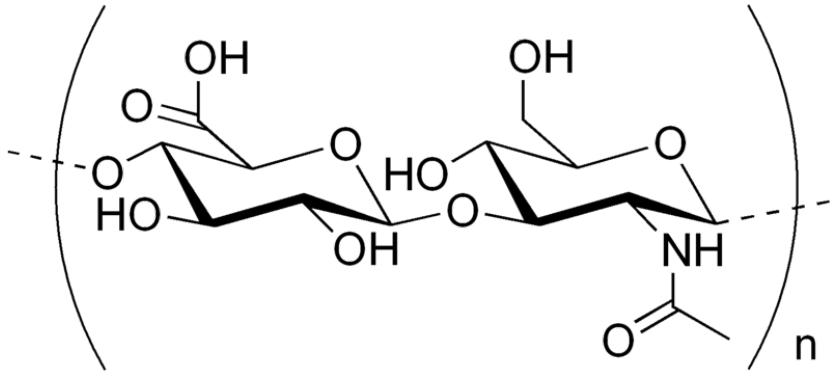

Figure 1: the molecular structure of Hyluronic Acid.

It is soluble in water and behaves as a weakly charged polyelectrolyte due to the carboxylic function presents on both disaccharide units.

It's widely accepted that HA conformation and structure in water, underlie most of its physical-chemical properties that allowing to control both physiological and biomedical functions, useful in human and veterinary surgery[3]. HA, indeed, has strong multiple interactions with water and within its structure that are responsible for its elevated excluded volume, enhanced viscoelastic properties, and probably also influence the interaction with cells[3].

The conformation of HA is sensitive to its electrolyte environment. Usually increasing quantities of the salt carries out a structure contractions; its conformation, indeed, is sensitive to the salt

concentration, and in excess of salt it behaves as a neutral polymer in a good solvent [4].

In no salt conditions, i.e. neutral case, the behaviour of HA solutions at different polymer concentrations, is leaded by interactions of its chains. In fact increasing the value of HA concentration, the polymer chains overlap each other, and exceeding a value of a critical overlap concentrations, the network shows a marked viscoelasticity properties; this results, indeed, are also function of the molecular weight of the polymer.

Accurate studies of the HA solutions have been performed with widespread techniques. About the understanding of molecular structures was executed measurements of Small Angle Neutron Scattering (SANS)[6]

Investigations of transport phenomena with probes dispersed in HA solutions and rheological measurements were performed: indeed both have provided an helpful information about the dynamic response of these material.[7]

De Smedt et al investigated the network structure of HA dispersing a dextrans, labelled with a fluorescent probe, and measuring the mobility through the Fluorescent Recovery After Photobleaching (FRAP)[7]. These measurements allows them to estimate the structural parameter of the network, as the mesh size of the polymer, the average distance between neighbouring strands of polymer [8]. This mesh is estimated in a range varying from 10 and 100 nm, in agreement with values calculated by other techniques[4].

In the FRAP information there are evidence of no chain-chain association among the polymer chain such as hydrophobic interaction. The flexibility and permeability properties of HA network can be

accounted for in terms of inter-chain hydrodynamic interaction such as entanglement.

Here, we investigate the diffusion properties of anisotropic particles of ellipsoidal shape in HA solutions at several concentrations spanning the whole transition among the dilute, semidilute and entangled regimes.

A comparison of the diffusion properties of polystyrene particles, dispersed in these solutions, is carried out for several particles of different shapes. Stretched particles were obtained from spherical particles after deforming a polymeric film in which particles are dispersed. The procedure leads to ellipsoids with different stretching ratios. The diffusive comparison was studied in terms of the mean square displacement analysis, calculated with the particle tracking technique.

3.2 MATERIALS AND METHODS

3.2.1 Polymer solutions:

Hyaluronic acid solutions (HA) with average molecular weight of 155 KDa were prepared in different concentrations. HA powder (Fidia Biopolymers) was dissolved in ultra pure milli-Q water at stock concentration of 10 mg/ml. The stock solution was slowly stirred for more than 24 hours. By successive dilution was prepared 10 solution at this concentration: 0.1, 0.3, 0.6, 1.0, 1.3, 1.5, 3.0, 6.0, 9.0 mg/ml.

3.2.2. Ubbelohde Viscometer:

On the polymeric solution viscosity measurements are performed, using a Ubbelohde Viscometer (Cannon Instruments). The solution are

loaded in viscometer and put in thermostatic conditions by a water reservoir at standard ambient temperature condition (293 K, 1 atm).

The solution are charged in the reservoir of the viscometer. Then the liquid is pumped through the capillary and loaded in measuring bulb, using a supplementary pressure inflates by the hand pump.

After that releasing the supplementary pressure, at the polymer solution is allowed to travel back through the measuring bulb and the time it takes for the liquid to pass through two calibrated marks is a measure for viscosity.

3.2.3 Preparation of colloidal ellipsoids:

Ellipsoid particles shape were prepared starting from spherical particle of 88 nm diameter. The procedure to obtain this ellipsoid consists in heating the spherical shape particles dispersed in polymer film, at a temperature T>Tg, and successively stretching this film.

In first time a 10% (wt/vol) solution of Poly Vinyl Alcohol PVA (Sigma-Aldirch) were prepared. This polymer were dissolved in 40 ml of milli-Q water at 85 °C temperature. Then, 2% (wt/vol) glycerol (Sigma-Aldrich) was added to a polymer solution to plasticize and reduce the Tg of the films. Successively spherical green particle of 88 nm (Duke Scientific), probed with a fluorescent dye, was suspended in this mixture in a concentration of 0.7% (wt/vol). Then the polymer solution was laid down in flat surface Teflon mold of 19 x 24.5 cm area with a thicknesses of 70 um. After 24 hours and more the water component evaporates, living a solid film less than a millimetre of thickness. The film was cut in 5 cm stripes and mounted in aluminium clamps of the stretcher (Instron). Inside the stretcher chamber film was heated at temperatures comprise between 120 and 150 °C and stretched at 0.3-05 mm/s rate.

Different stretching ratio was adopted (2.5, 3.8 and 4.5 times the length of the relaxed film).

After stretching procedure the elongated particles from PVA film was recovered; indeed it was dissolved in a mixture of 35% isopropanol and 65% water. After that, the solution was centrifuged and washed ten times with same alcoholic mixture to eliminate the PVA traces.

A Scanning Electron Microscopy (SEM) analysis was performed to check the ellipsoidal shape and the experiment success. SEM image is reported in Figure 2

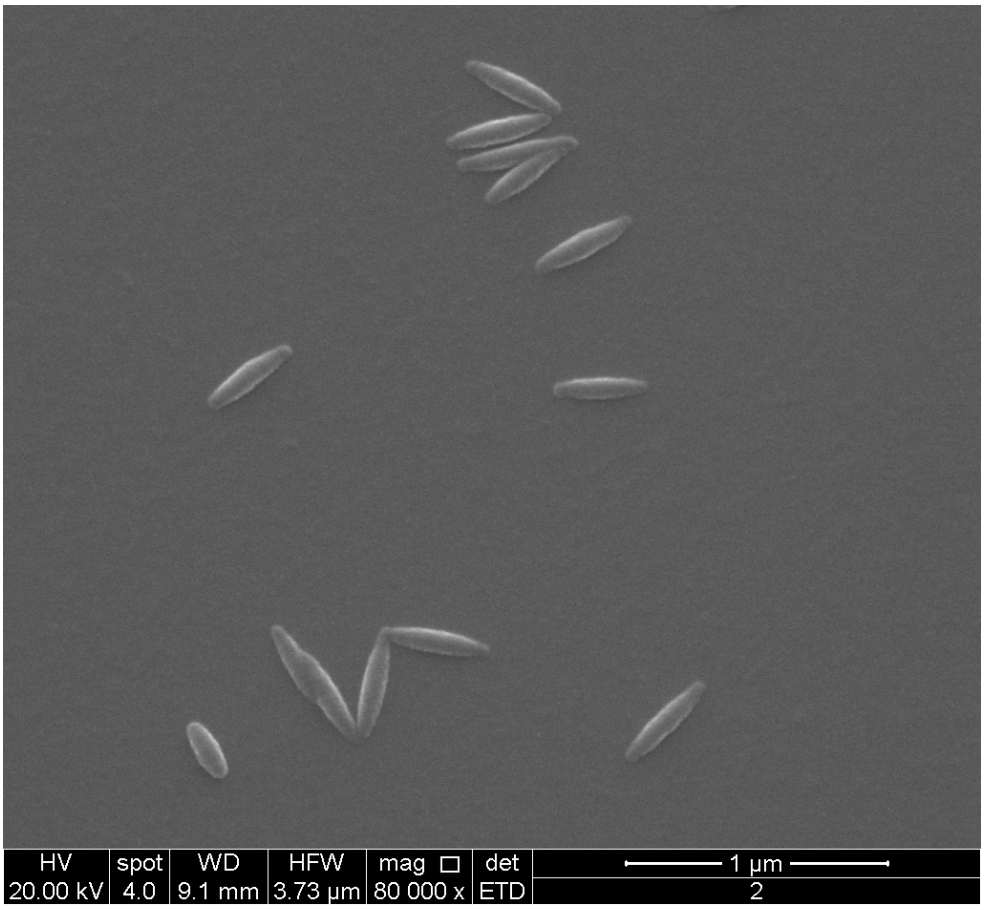

Figure 2: Scanning Electron Microscopy of nano particle stetched from 88 nm radius nano bead. The stretching ratio is 4.8.

3.2.4 Particle dispersion:

Latex colloidal particles, in spherical and in ellipsoidal shapes, were dispersed in HA solution at different concentration. The particle polymer ratio is about 0.05 % (volume/volume). Once the particle was added to the HA solutions, the suspension was sonicated for a few minutes to avoid particle aggregation.

3.2.5 Microscope, fast camera and video sequences:

The instrument used was the Olympus X81 inverted microscope with an Olympus 100x Uplsapo 1.4 numeric aperture objective. The illumination was given by a Hg lamp emitting a continuous spectra. A dichroic filter was used to select an opportune wave length of 480 nm in excitation and 520 nm in emission.

The sample, particle suspensions, in the chamber slide was loaded.

The image sequences were recorded with Hamamatsu Orca Flash 4.0. This CMOS technology camera allows to record a stack of images of 512 x 2048 pixels at a frame rate of 400 fps corresponding to a time window of 0.0025 s acquisitions. The pixel size of this camera is 6.5 um and this value, coupled to 100x optics, allows to obtain a pixel resolution of 0.065 micron/pixel.

For each concentration of HA 5 video sequence of 3000 frame were performed. In each frame are present an average number of about 70 particles, collecting more than 10^6 Brownian jumps. All video sequences were sampled in different xy positions of the camber slide. The focus position was fixed at least to 10 μm up the bottom of the chamber, avoiding the hindrance effect of the slide floor.

3.2.6 Data analysis

The software used for a particle was Eclipse, a free licence IDL compiler. The script package, and relative tutorial, is available at web page of Harvard University: [9]

In the tracking analysis a parameter of a minimum distance of separation, about 4 μm, between each particle couples was adopted: indeed frame with particles closer than this distance are neglected. Only trajectories with at least 10 continuous jumps were selected, deleting shorter paths. The mean square displacement was extract from matrix track and saved in a set of file for different concentration of HA. This data was exported in text file and successively fitted. It was plotted the mean square displacements as function of time. Data were fitted in the linear range, from 0.01 s to 0.3 s.

3.3 RESULTS AND DISCUSSION

The polymer studied is HA of 155 kD. Viscosity and diffusion measurements were performed at different concentrations of the polymer. The knowledge of these parameters allows the understanding of dynamic and structural properties of HA solutions. Moving form 0.1 mg/ml to the 9 mg/ml it has been possible exploring a wide range of viscosities.

The increasing of the concentration corresponds to an increase of viscosity. This evidence is represented in the plot of figure 3a, where the relative viscosity in function of the concentrations is reported

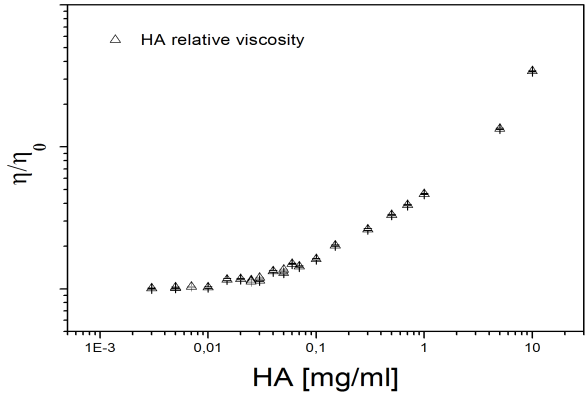

Figure 3a: The relative viscosity at different concentration of HA

The dependence of viscosity upon the concentration can be distributed in three different regions, corresponding to different regimes of solution: dilute, semi-dilute and entangled regime. In all concentrations the data obtained by the Ubbelohde viscometer are fitted by the power low [4]:

$$\eta = Bc^A \qquad (1)$$

In the low concentration (the dilute regime) the data can be fitted with a curve having $A \approx 1$. Afterward c^* concentration (overlap concentration) the semi-dilute regime is predicted. The polymer chains interactions give rice to an increasing viscosity, and the power law exponent in the power low changes, with $A \approx 0.5$. Increasing the concentration the third regime is reached. At c^e (entanglement concentration) the viscosity increase and the value of the power law exponent is $A \approx 1.5$. This data are obtained by the intersection of three green lines in figure 3b. This plot represents the specific viscosity:

$$\eta_{sp} = \frac{\eta}{\eta_0} - 1 \qquad (2)$$

The relative ratio of the c^* and c^e are $\approx$ 0.1 mg/ml and $\approx$ 1.0 mg/ml. The $c^e \approx 10c^*$ in according with Colby and Rubinstein theory[4].

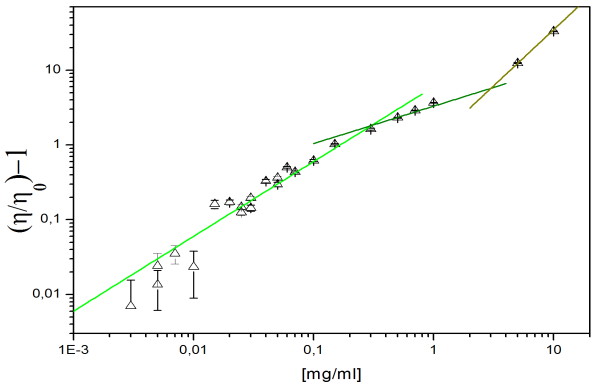

Figure3b: Ubbelohde measurements of viscosity at several HA concentrations. Lines represent power low regressions.

The analyses of the mean square displacements are useful to understand the diffusion processes of nano particles dispersed inside the polymer mesh, as to understand local properties of the polymer and reckon differences in nano-viscosities and macro-viscosities. We conducted several measurements in salt free solutions. The probe size chosen is comparable, as order of magnitude, with the polymer mesh size; the spherical latex particles are indeed 88 nm in diameter and are functionalized with fluorescein molecules.

We tracked the mobility of different particles having different stretching ratios in HA solutions in dilute, semidilute and entangled regimes. The SRs (stretching ratios) obtained are 2.5, 3.8, 4.8.

The time window τ selected in the fitting data corresponds to a linear behaviour region, where a unit slope represents a classical diffusive regime. Short time values of the MSD are not taken into account: indeed, these times might correspond to elastic behaviour of the polymer. In

high viscosity solutions the mobility of the particle is reduced and each particle can be tracked for a long time window while the same is not possible for low viscosity solutions experiments.

The equation of the curve used to fit the data is:

$$\Delta^2(\tau) = 2dDt + \Delta_0^2 \qquad (3)$$

The additive quantity Δ_0^2 contains the error due to the short time diffusion and to measurement errors ($2d\Delta_\epsilon^2$). The negligible linear deviation of the fitting is due to the effect of the caging in the dense suspension [9].

Fitted data at each stretching ratio are reported in the figure 4:

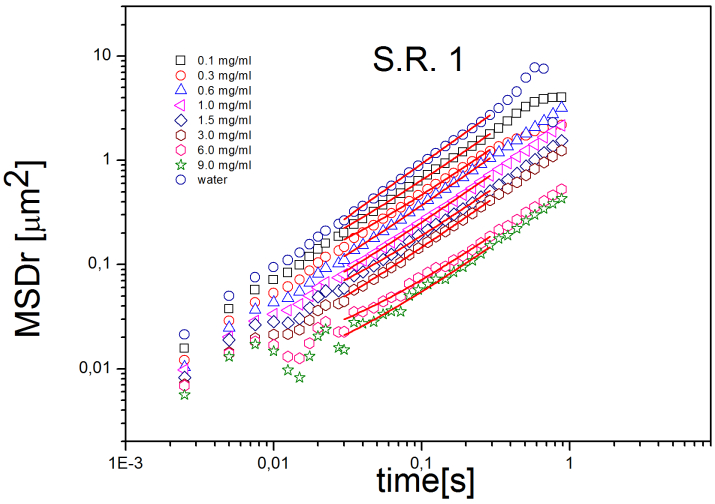

Figure 4a: Fitting of Mean Square Displacement of the nano particle with stretching ratio1

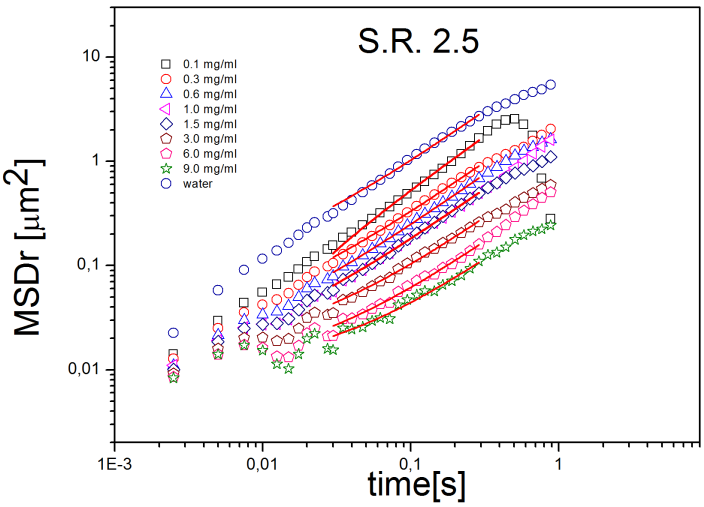

Figure 4b: Fitting of Mean Square Displacement of the nano particle with stretching ratio 2.5

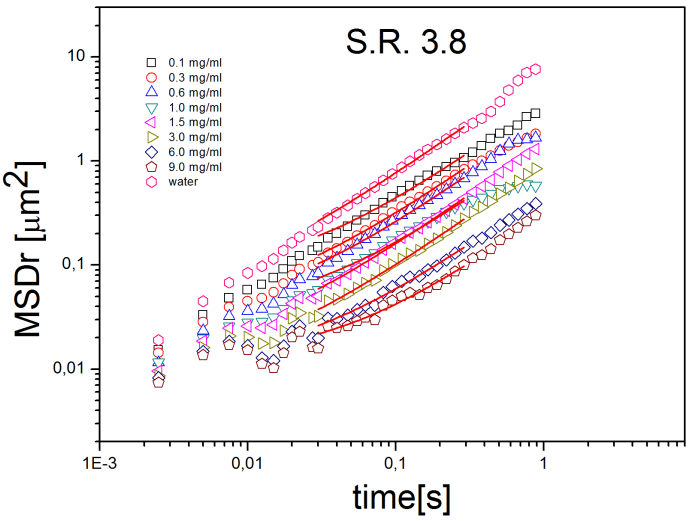

Figure 4c: Fitting of Mean Square Displacement of the nano particle with stretching ratio 3.8

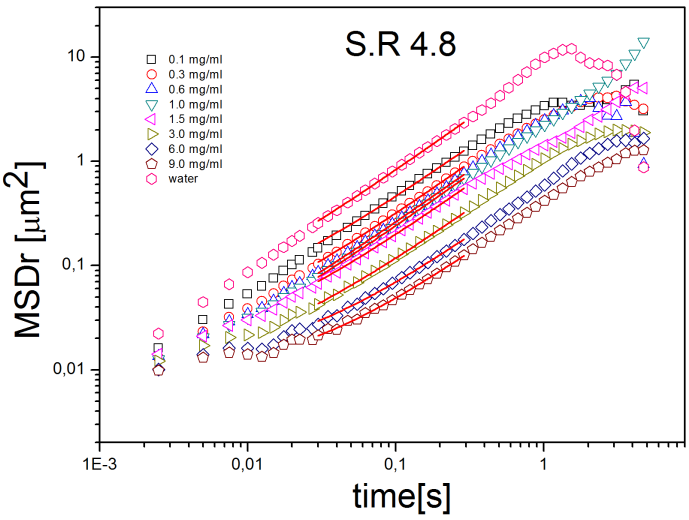

Figure 4c: Fitting of Mean Square Displacement of the nano particle with stretching ratio1

The values of the Diffusion coefficients evaluated for the four starching ratios at different HA concentrations are compared. For all four SRs, the diffusion coefficients decay with exponential trends with increasing HA concentration, as reported in the figure 5:

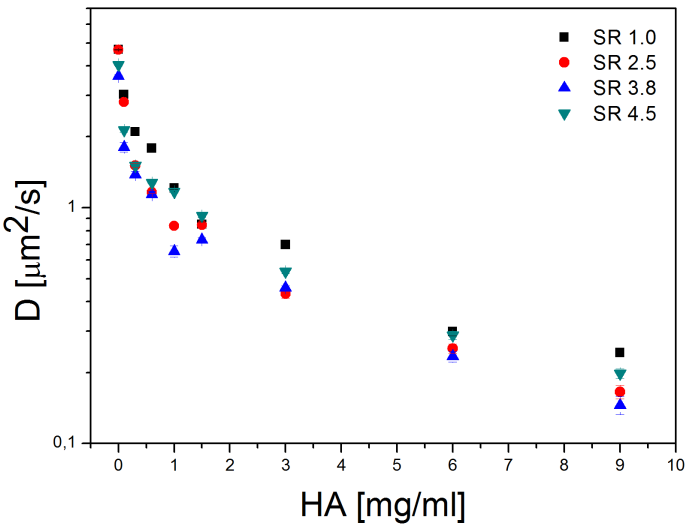

Figure 5: diffusion coefficients of four different stretching ratio nano particle in different hyaluronic acid concentrations

In particular, the greater percentage of the diffusion coefficient reduction takes place within the semi-dilute regime. In figure 6 is reported the normalized diffusion coefficient respect to the diffusion coefficient evaluated in the pure solvent:

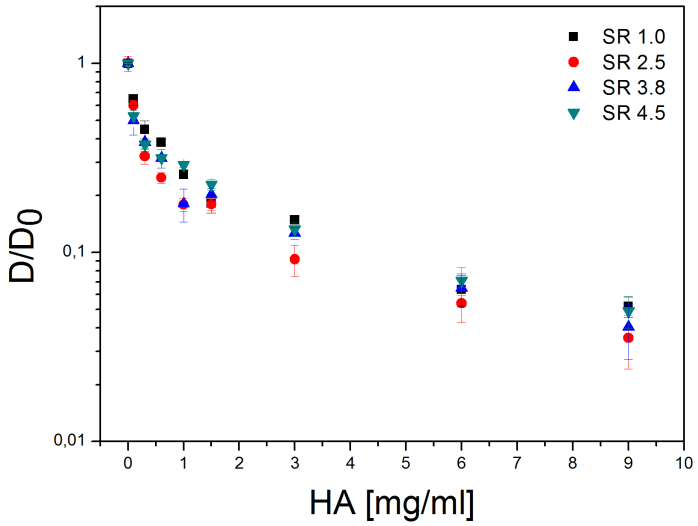

Figure 6: The normalized diffusion coefficient respect to the diffusion coefficient in the water

The value of D/D_0 deviates from unity of a factor of 80% at the c*. The spare part of the decays takes place in the entangled regime.

In Figure 7 we report the comparison between the normalized values of the Diffusion coefficients of each ellipsoids over the diffusion coefficient of a sphere of equal size in water.

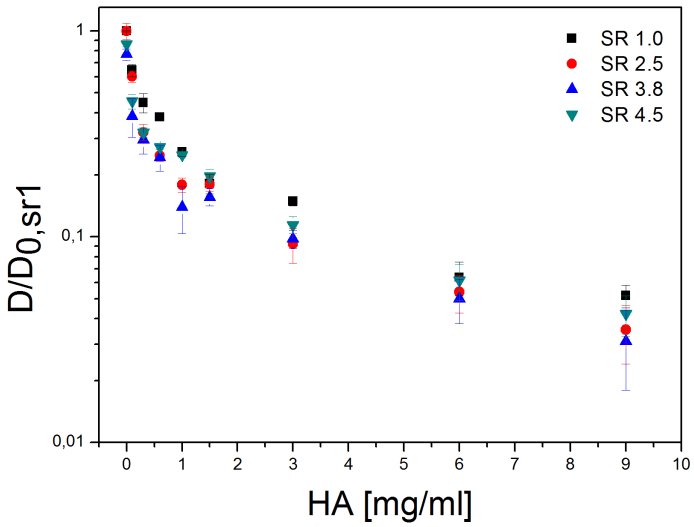

Figure 7: The normalized diffusion coefficients over to the diffusion coefficient in the water of the equal size spherical particle

The diffusion of the sphere is obviously greater than that of a stretched particle. Interestingly, in the transition from the semi-dilute to the entangled regime the high ratio ellipsoid (S.R. 4.8) recovers the diffusion coefficient values of the sphere.

A theoretical equivalent hydrodynamic radius was calculated for the ellipsoid.

The equivalent diameter of an ellipsoid can be calculated according with the Heyt & Diaz formula[10]:

$$de = 1.55\, A^{0.625} / P^{0.25} \qquad (4)$$

where

A = cross-sectional area of ellipsoid (nm^2)

P = perimeter of ellipsoid (nm^2)

These geometric parameters are represented in figure 8:

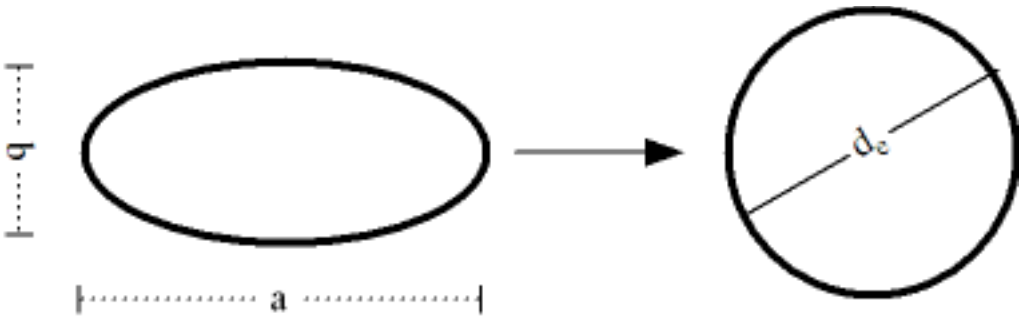

Figure 8: geomoetric representation of ellipsoid parameter.

The cross-sectional area of an oval ellipsoid could be expressed as

$$A = \frac{\pi a b}{4} \qquad (5)$$

where:

a = major dimension of the flat ellipsoid [nm]

b = minor dimension of the flat ellipsoid [nm]

The perimeter of an ellipse can be approximated to

$$P \approx 2\pi\sqrt{\left(\frac{1}{2}\left(\frac{a}{2}\right)^2 + \left(\frac{b}{2}\right)^2\right)} \qquad (6)$$

and the equivalent diameter can be expressed by:

$$d_e = 1.55\frac{\left(\frac{\pi b^2}{4} + ab - b^2\right)^{0.625}}{(\pi b + 2a - 2b)^{0.25}} \qquad (7)$$

The equivalent hydrodynamic radius for each stretching ratio is reported in table 1.

Stretching Ratio	X-Axis [nm]	Y-Axes [nm]	R_h [nm]
1	88	88	44
2.5	246	53	50.8
3.8	334	45	52
4.8	414	40	52.7

Table 1: Major and minor dimension and hydrodynamic radius for different stretched nano particle

At this point is interesting to compare the local nano viscosities obtained from the particle tracking measurements with the macroscopic viscosities measured with the Ubbelodhe viscometer.

Knowing the diffusion coefficient calculated by particle tracking technique and the hydrodynamic radius of the spherical and elliptic particles, the Stokes Einstein relation gives the viscosity. This value is lower than the macroscopic viscosity, indeed the ratio between the two values is lower than unity. In particular, in the dilute and semi dilute regimes the nano-viscosity measured is far lower than the macroscopic value for all particles. The value of nano viscosity evaluated is less than 50% of the macroscopic one (figure 9). This effect may be due to the relative large mesh size of the polymer chain. Indeed probes may explore an environment much similar to the solvent, since polymer chains are quite far one from the other. Interestingly the ratio becomes almost unity at the crossover with the entangled regime, while for $c > c_e$ particles again explore a diffusive media having lower viscosity than the macroscopic value obtained. In particular, the viscosity ratio measured with the SR 4.8 ellipsoid is lower respect to the others in the entangled

regime. This could be attributed to a preferential disentanglement orientation of the highly elongated particle.

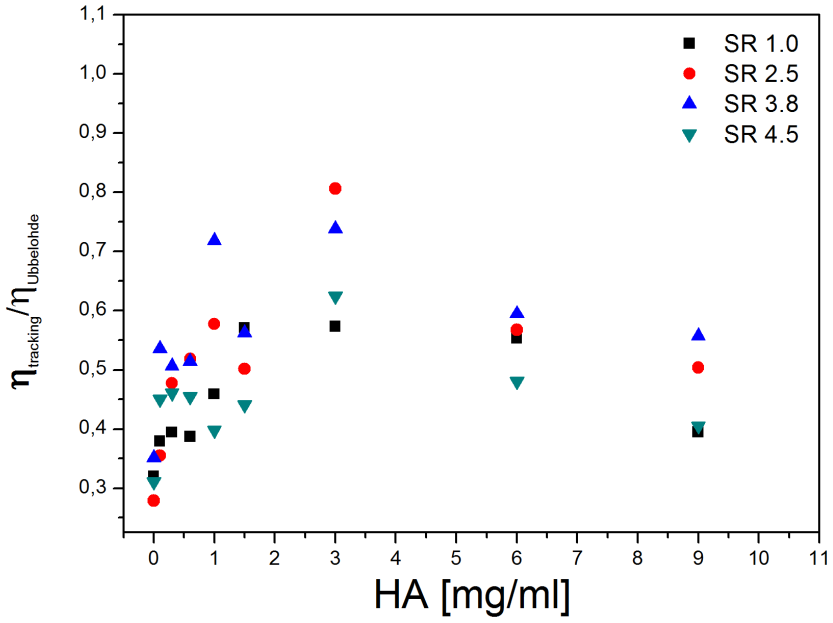

Figure 9: the ratio between the nano viscosity and micro viscosity

3.4 CONCLUSION

In this paper it has been addressed an introduction of the diffusion problems in the polyelectrolyte solution of HA in water. The macroscopic viscosity is analysed for a wide range of HA concentrations. All regimes are explored: dilute, semidilute and entangled. The intersections of the specific viscosity fittings correspond to the overlap and entangled concentrations. These values are in good agreement with the theoretical expectations for polyelectrolytes[4]. Measurements of the diffusion coefficients for spheres and ellipsoids of various stretching ratios (SRs) were obtained through particle tracking in HA solutions. By increasing

the Ha concentration a lower diffusion coefficient is measured independently of the particles shape. The greater percentage of the diffusion coefficient reduction takes place before the entangled concentration c_e. The comparison of diffusion coefficients among different SRs gives ideas of the "*shape effect*". The diffusion of the sphere is usually greater than that of a stretched particle. A theoretical hydrodynamic radius for the ellipsoids is calculated and through the Stokes Einstein equation, a value of nano viscosity was found. A comparison between nano viscosities and macro viscosities for different SRs ratios was performed at different concentrations with values of nano viscosities slightly lower than micro viscosities. After the entangled concentration, the elongated particles probe a lower value of viscosity compared to other less elongated particles.

REFERENCES

[1] Shenoy, V ; Rosenblatt, J, Macromolecules,28, 26, 8751-8758(1995)

[2] Rapport, M . M., Weissman, B, Nature, 1951,168,996

[3] Balazs, E. A., In viscolestic materials: Basic science and clinical apllication,; Rose, E., Ed.; Pergamon Press, Oxford, U.k.,(1998)

[4] Dobrynin, A. V., Colby, R. H., Rubinstein, M., Macromolecules, 28, 1859-1871 (1995)

[5] (Morfin, I, Buhler, E, Cousin, F.,Grillo, I, Boue, F, BIOMACROMOLECULES, 12,4,859-870 (2001))

[6] De Smedt, S.C., Lauwers, A., Demeester, J, Macormolecules, 27,141-146, (1994)

[7] http://www.uni-leipzig.de/~pwm/web/?section=introduction&page =polymers (last access 12/2013)

[8] http://weitzlab.seas.harvard.edu. (last access 12/2013)

[9] J. C. Crocker and D.G. Grier, journal of colloid and interface science 179, 298–310 (1996)

[10] http://www.engineeringtoolbox.com/equivalent-diameter-d_205.html (last access 12/2013)